Cell Reports

Article

Plakophilin 3 facilitates G1/S phase transition and enhances proliferation by capturing RB protein in the cytoplasm and promoting EGFR signaling

Graphical abstract

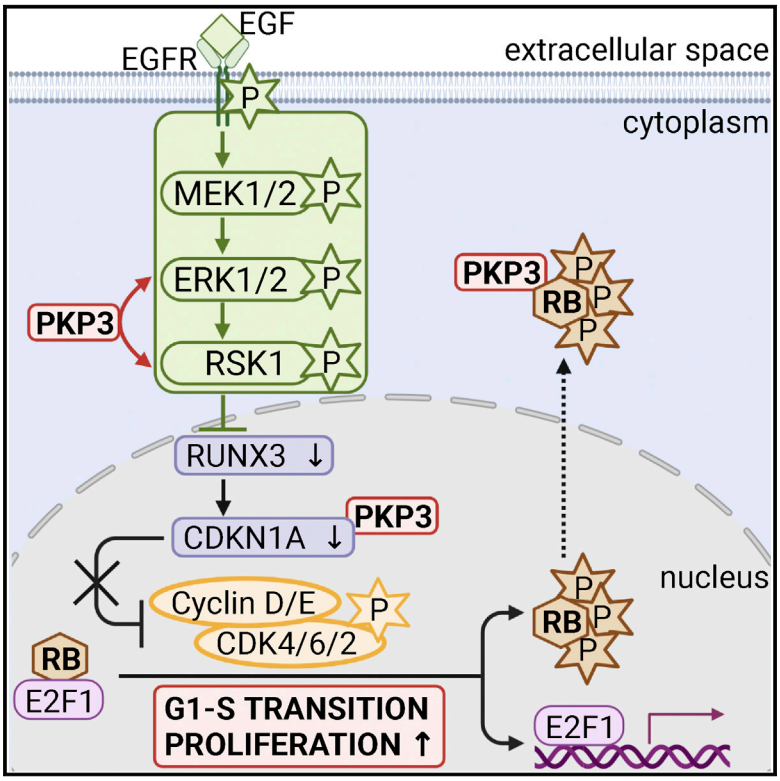

Highlights

- PKP3-expressing cells reveal higher proliferation rates
- PKP3 captures hyper-phosphorylated RB in the cytoplasm
- This increases E2F activity and promotes G1/S phase transition
- Upstream of RB, PKP3 increases mitogenic signaling via ERK and RSK

Authors

Lisa Müller, René Keil, Mechthild Hatzfeld

Correspondence

lisa.mueller@uk-halle.de (L.M.), mechthild.hatzfeld@medizin.uni-halle.de (M.H.)

In brief

Müller et al. elucidate plakophilin 3's (PKP3) functions in proliferation. (1) PKP3 serves as a scaffold for ERK and RSK to enhance mitogenic signaling. (2) PKP3 directly promotes cell-cycle progression by capturing and inactivating the tumor-suppressor protein RB. This provides insights into PKP3's role in cancer.

Müller et al., 2023, Cell Reports *42*, 112031
January 31, 2023
https://doi.org/10.1016/j.celrep.2023.112031

CellPress

Cell Reports

CellPress
OPEN ACCESS

Article

Plakophilin 3 facilitates G1/S phase transition and enhances proliferation by capturing RB protein in the cytoplasm and promoting EGFR signaling

Lisa Müller,[1,*] René Keil,[1] and Mechthild Hatzfeld[1,2,*]
[1]Charles Tanford Protein Research Center, Martin Luther University Halle, Institute of Molecular Medicine, Department for Pathobiochemistry, Kurt-Mothes-Str. 3A, 06120 Halle, Germany
[2]Lead contact
*Correspondence: lisa.mueller@uk-halle.de (L.M.), mechthild.hatzfeld@medizin.uni-halle.de (M.H.)
https://doi.org/10.1016/j.celrep.2023.112031

SUMMARY

Plakophilin 3 (PKP3) is a component of desmosomes and is frequently overexpressed in cancer. Using keratinocytes either lacking or overexpressing PKP3, we identify a signaling axis from ERK to the retinoblastoma (RB) protein and the E2F1 transcription factor that is controlled by PKP3. RB and E2F1 are key components controlling G1/S transition in the cell cycle. We show that PKP3 stimulates the activity of ERK and its target RSK1. This inhibits expression of the transcription factor RUNX3, a positive regulator of the CDK inhibitor CDKN1A/p21, which is also downregulated by PKP3. Elevated CDKN1A prevents RB phosphorylation and E2F1 target gene expression, leading to delayed S phase entry and reduced proliferation in PKP3-depleted cells. Elevated PKP3 expression not only increases ERK activity but also captures phosphorylated RB (phospho-RB) in the cytoplasm to promote E2F1 activity and cell-cycle progression. These data identify a mechanism by which PKP3 promotes proliferation and acts as an oncogene.

INTRODUCTION

Cell-cell junctions are essential for the maintenance of tissue morphogenesis and homeostasis.[1,2] Desmosomes are highly specialized junctions that mediate strong adhesion. Accordingly, they are found in tissues that are exposed to high mechanical stress, such as the heart and skin. Nevertheless, epidermal desmosomes of the basal layer must be dynamic to enable proliferation, which is necessary for tissue regeneration and renewal.[3] Beyond the structural functions required for tissue resilience, desmosomal proteins participate in numerous signaling pathways affecting inflammation, differentiation, cell survival, and proliferation.[4]

The plakophilin (PKP) family members PKP1, PKP2, and PKP3 have a tissue- and cell-type-specific expression pattern. PKPs are indispensable regulators of desmosomal adhesion by linking the desmosomal cadherins with the desmosomal plaque proteins plakoglobin and desmoplakin. PKPs are also involved in the regulation of transcription, translation, mRNA metabolism, migration, and proliferation.[5,6] PKP3 is present in the desmosomes of most epithelial cells and is regulated by the epidermal growth factor receptor (EGFR) signaling pathway. Activation of this pathway promotes PKP3 phosphorylation and localization at keratinocyte tricellular contacts that are important for the control of cell dynamics during tissue homeostasis and repair.[7] The extra-desmosomal functions of PKP3 are not well characterized. In the cytoplasm, PKP3 interacts with RNA-binding proteins[8] or the 14-3-3 protein stratifin.[9] In prostatic adenocarcinoma cells, overexpression of PKP3 exhibits desmosomal and cytoplasmic localization with an increase in cell proliferation rates.[10] In non-small cell lung carcinoma, increased PKP3 expression correlated with poor prognosis and reduced survival. In these cells, PKP3 knockdown reduced cell growth.[11] Based on a putative cancer-promoting role of PKP3, its mRNA was proposed as a biomarker for the detection of circulating cells in the blood of patients with gastrointestinal or ovarian cancer.[12,13] These data suggest that PKP3 promotes proliferation. However, the role of PKP3 in cancer seems to be context dependent,[6] and the molecular mechanism by which PKP3 may modulate proliferation is still unclear in both transformed and non-transformed cells.

Although several desmosomal proteins have been reported to modulate proliferation, the underlying molecular mechanisms are largely unknown. Here, we describe how PKP3 promotes cell-cycle progression and proliferation by controlling retinoblastoma (RB) phosphorylation in non-transformed keratinocytes. Through PKP3-dependent stimulation of the canonical EGFR-ERK-RSK1 axis, PKP3 suppresses Runt-related transcription factor 3 (RUNX3) and its transcriptional target, CDKN1A. This releases CDKN1A-mediated inhibition of RB phosphorylation and promotes E2F1 activation. By sequestering phosphorylated RB in the cytoplasm, PKP3 further increases E2F1 target gene transcription, leading to accelerated progression from G0/G1 to S phase, thereby increasing proliferation.

RESULTS

PKP3 affects the proliferation and differentiation of keratinocytes

Several studies have reported elevated expression of PKP3 in cancer cells, suggesting a role of PKP3 in promoting proliferation. However, how PKP3 affects proliferation at the molecular level is not known. We investigated whether PKP3 affects the proliferation rate in non-transformed epidermal keratinocytes. As a model system, we used murine wild-type (WT) keratinocytes, PKP3-knockout (PKP3-KO) keratinocytes, and WT keratinocytes overexpressing PKP3-GFP (WT + PKP3).[14]

Cell proliferation was tracked using an IncuCyte S3 system. The area occupied by nuclei was monitored for 4 days. Supporting our hypothesis, growth rates differed between WT, PKP3-KO, and WT + PKP3 cells (Figure 1A). WT and WT + PKP3 cells had similar growth patterns with continuous proliferation, as indicated by a steep ascent of the relative area occupied by nuclei. Up to day 3, their proliferation appeared indistinguishable. After 3 days, however, a flattening of the curve revealed a tendency of WT cells to become non-proliferative when reaching high density, whereas WT + PKP3 cells continued to proliferate, suggesting that these cells are able to overcome density-dependent inhibition. Loss of PKP3 resulted in a flat curve even after 96 h, suggesting that PKP3 promotes proliferation in untransformed keratinocytes.

To determine more directly which phase of the cell cycle was primarily affected, the proportion of cells in G0/G1, S, and G2 phase/mitosis was measured by flow cytometry. This analysis showed an enrichment of PKP3-KO cells in G0/G1 and a reduction of WT + PKP3 cells in this phase (Figure 1B). To further validate these data, cells were grown in low- or high-Ca^{2+} medium (LCM or HCM, respectively). Reduced confluence of PKP3-KO cells was visible at 72 h in LCM and HCM (Figure S1A). Flow cytometry confirmed increased numbers of PKP3-KO cells in G0/G1 phase even after WT and WT + PKP3 cells had reached confluence (Figure S1B).

The fluorescence ubiquitination cell-cycle indicator (FUCCI) technology is based on the expression of two proteins that show cell-cycle-regulated oscillations (Figure S1C). Fluorescence of WT and PKP3-KO cells stably expressing FUCCI probes was analyzed using the IncuCyte S3 system. This allowed cell-cycle progression to be monitored at the single-cell level. The loss of PKP3 prolonged the G1 phase approximately 2-fold compared with WT keratinocytes, whereas other phases of the cell cycle were unaffected (Figure 1C). This considerable enrichment of PKP3-KO cells in G0/G1 suggested a delay in S phase entry.

To compare the number of cells in S phase, we measured the incorporation of 5-bromo-2′-desoxyuridine (BrdU) into newly synthesized DNA. BrdU incorporation was significantly decreased in PKP3-KO cells, indicating a decrease in the number of cells in S phase, whereas WT + PKP3 cells showed a moderate increase in BrdU incorporation at 72 h (Figure 1D). This finding correlates with the growth curves and further supports a delay in the G1/S phase transition in PKP3-KO keratinocytes.

In the basal layer of the epidermis, keratinocytes proliferate but start to differentiate upon stratification. Thus, proliferation and differentiation are typically inversely correlated. When cells stop proliferating, they can either irreversibly withdraw from the cell cycle to proceed to a terminally differentiated state or enter the quiescent (G0) phase, from which the cells can reenter the cell cycle. Quiescence is an important feature of many types of stem cells.[15] The expression of differentiation-specific markers enables quiescence and differentiation of epidermal cells to be distinguished. Early epidermal differentiation is characterized by increased expression of desmoglein 1 (DSG1), keratin 1 (KRT1), and KRT10 in the spinous layer of the epidermis, whereas corneodesmosin (CDSN), involucrin (INV), and loricrin (LOR) are expressed in the upper corneal and granular layers (Figure S1D). To examine whether reduced proliferation correlates with increased differentiation in PKP3-KO cells, we analyzed the expression of several differentiation markers (Figure 1E). Keratinocytes were cultured for 72 h in either LCM or HCM to induce differentiation. Ca^{2+} treatment in PKP3-KO cells resulted in unaltered or decreased expression of differentiation markers compared with WT cells. This demonstrates that growth retardation in PKP3-KO cells is not a consequence of premature differentiation.

Taken together, the results show that loss of PKP3 resulted in an enrichment of cells in G1 phase and a retardation of S phase entry, indicating that PKP3 facilitates proliferation and cell-cycle progression.

PKP3 promotes E2F1 activity

RB is an essential regulator of G1/S phase transition (Figure 2A). Mitogenic signals induce the synthesis of cyclins D and E, which form complexes with CDK4/CDK6 and CDK2, respectively. These activated complexes promote RB phosphorylation. Non-phosphorylated RB associates with E2F1, which suppresses its transcriptional activity during early G1 phase. Mono-phosphorylation of RB by the cyclin D-CDK4/CDK6 complex and hyper-phosphorylation by the cyclin E-CDK2 complex inactivates RB in late G1 phase. Hyper-phosphorylated RB dissociates from E2F1 to allow transcription of E2F1 target genes that promote G1/S phase transition.

To analyze the putative effect of PKP3 on the RB pathway, we quantified the amount and activation of several proteins involved in this pathway by immunoblotting (Figure 2B). Expression of cyclins D1, D2, and E was unaltered in PKP3-KO cells. Moreover, the level and activation of CDK4 (i.e., phosphorylation at Thr172) were not affected by the loss of PKP3. However, PKP3-KO cells had reduced CDK6 abundance and Tyr24 phosphorylation, suggesting a low level of inactive CDK6. Despite its reduced expression, activation of CDK6 by phosphorylation at Thr177 was similar in WT, PKP3-KO, and WT + PKP3 cells. In contrast, the CDK2 protein level was significantly increased in PKP3-KO cells, but the amount of activated CDK2-phosphorylated Thr160 (phospho-Thr160) was unaltered. WT + PKP3 cells had decreased CDK2 levels without a decrease in activation (Figure 2B). Thus, PKP3 appears to affect the expression of CDK6 and CDK2 without significant effects on their activation.

Although, PKP3 did not affect the activities of the cyclin-CDK complexes upstream of RB, we observed a remarkable reduction of phospho-RB (Ser 807/811) in PKP3-KO cells, whereas WT + PKP3 cells had elevated levels of phospho-RB (Figure 2B; for validation of the phospho-RB antibody, see Figure S2A).

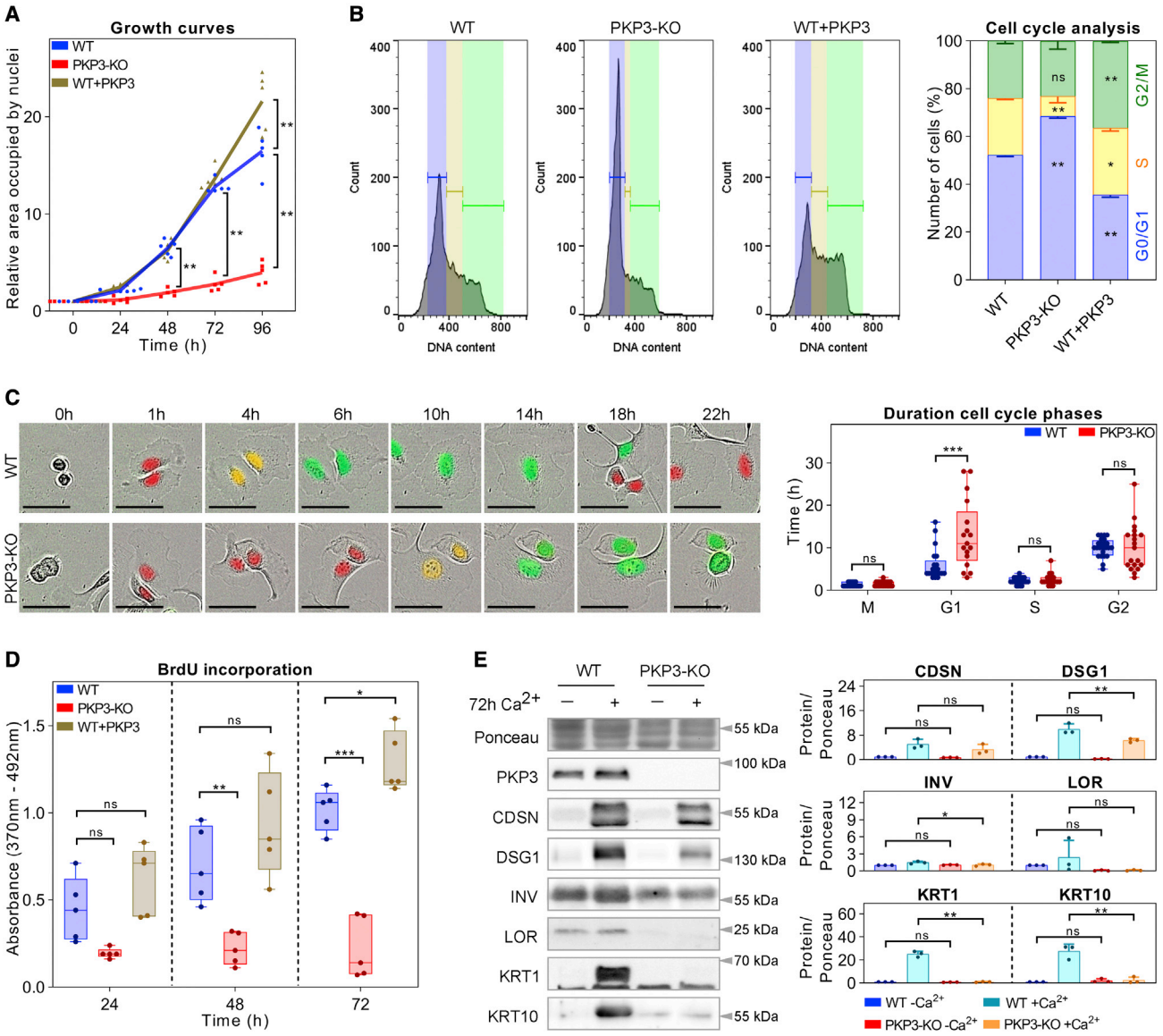

Figure 1. PKP3 affects the proliferation and differentiation of keratinocytes

(A) Area occupied by cell nuclei in WT, PKP3-KO, and WT + PKP3 keratinocytes at the indicated time points, as determined from live-cell images using an IncuCyte S3 system. Data are shown relative to measurements at the beginning of recording (time zero). Graphs represent average values from five independent experiments.

(B) Propidium iodide labeling and flow cytometry analysis of the cell cycle. Left: representative population histograms of the cell-cycle phase distribution for WT, PKP3-KO, and WT + PKP3 cells grown for 24 h in LCM. Blue, G0/G1 phase; yellow, S phase; green, G2/M phase. Right: the average + SD of three independent experiments is plotted.

(C) Cell-cycle phase duration determined using the FUCCI system. Left: representative images of WT and PKP3-KO FUCCI cells with segmentation mask overlays at the indicated time points. Red, G1 phase; yellow, S phase; green, G2 phase. Scale bars, 50 μm. Right: boxplots showing the duration of the cell-cycle phases in WT and PKP3-KO-FUCCI cells. Values from ≥17 cells per condition from ≥2 independent experiments are plotted. The whiskers extend to the minimum and maximum values.

(D) BrdU incorporation in WT, PKP3-KO, and WT + PKP3 cells grown for 24, 48, or 72 h in LCM. Boxplots show the absorbance from five independent experiments. The whiskers extend to the minimum and maximum values.

(E) Protein levels of differentiation markers in WT and PKP3-KO cells grown for 72 h in medium with or without Ca^{2+}. Left: representative immunoblot of PKP3 and epidermal differentiation markers. Ponceau S staining was used as a loading control. Right: quantification of protein amounts normalized to Ponceau S staining and relative to WT cells grown in medium without Ca^{2+}. Averages +S D from three independent experiments are plotted.

*p < 0.05; **p < 0.01; ***p < 0.001; ns, not significant. Significance was determined by one-way ANOVA with Tukey's multiple comparisons test (A, B, D, and E) or by Student's unpaired two-tailed t test (C).

See also Figure S1.

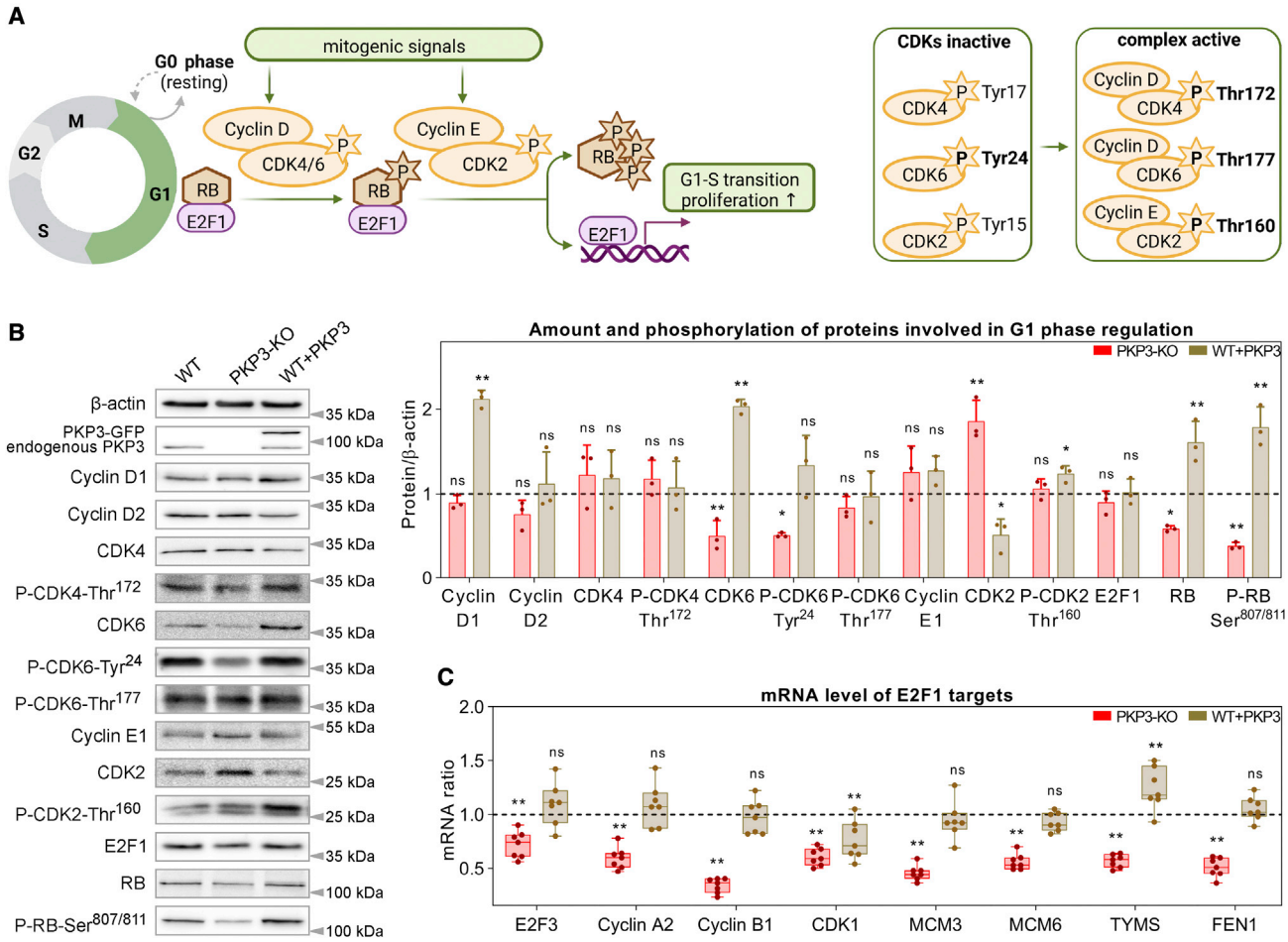

Figure 2. PKP3 promotes E2F1 activity

(A) Schematic of key events initiating G1/S phase progression (left) and CDK activation (right). CDK4/6 and CDK2 phosphorylation sites analyzed in (B) are marked in bold. Created with biorender.com.

(B) Amount and phosphorylation of proteins involved in G1 phase regulation. Left: representative immunoblot of proteins in WT, PKP3-KO, and WT + PKP3 cells. β-Actin was used as a loading control. Right: quantification of protein amounts and phosphorylation in PKP3-KO and WT + PKP3 cells normalized to β-actin and relative to WT cells. Averages + SD from three independent experiments are plotted.

(C) mRNA level of E2F1 targets in PKP3-KO and WT + PKP3 cells relative to WT cells. *Eif3k* was used as an invariant endogenous control (reference gene). Boxplots show the mRNA ratio from seven independent experiments. The whiskers extend to the minimum and the maximum values.

*p < 0.05; **p < 0.01; ***p < 0.001; ns, not significant. Significance was determined by one-way ANOVA with Tukey's multiple comparisons test.

See also Figure S2.

Since the altered amounts of total RB only partially account for the observed differences in RB phosphorylation, we conclude that PKP3 contributes to the regulation of RB phosphorylation.

To determine whether increased expression of CDK4 or CDK6 can rescue RB phosphorylation in PKP3-KO cells, we expressed hemagglutinin (HA)-tagged CDK4 or CDK6 in all three cell lines (Figure S2B). Neither the ectopic expression of CDK4 nor CDK6 increased RB phosphorylation in PKP3-KO cells, suggesting that reduced CDK6 expression is not a main driver of the prolonged G1 phase.

RB phosphorylation releases E2F1 to activate the transcription of cell-cycle-related genes and enables G1/S phase transition. E2F1 protein levels were not affected by PKP3 (Figure 2B). As RB phosphorylation was reduced in PKP3-KO cells, we hypothesized that E2F1 activity may also be reduced. To analyze the transcriptional activity of E2F1, we quantified mRNA levels of selected E2F1 target genes involved in cell-cycle control, such as *E2F3*; *CCNA2* (cyclin A2); *CCNB1* (cyclin B1); *CDK1*; DNA replication licensing factors *MCM3* and *MCM6*; thymidylate synthase (*TYMS*); and Flap endonuclease 1 (*FEN1*), by qRT-PCR. The levels were significantly decreased in PKP3-KO cells (Figure 2C), indicative of reduced transcriptional activity of E2F1. E2F1 target genes were essentially unaltered in WT + PKP3 cells, in agreement with indistinguishable growth rates of WT and WT + PKP3 cells for up to 72 h (Figure 1A).

Taken together, these data indicate that PKP3 promotes the G1/S phase transition by increasing RB phosphorylation, thereby enhancing E2F1 activity.

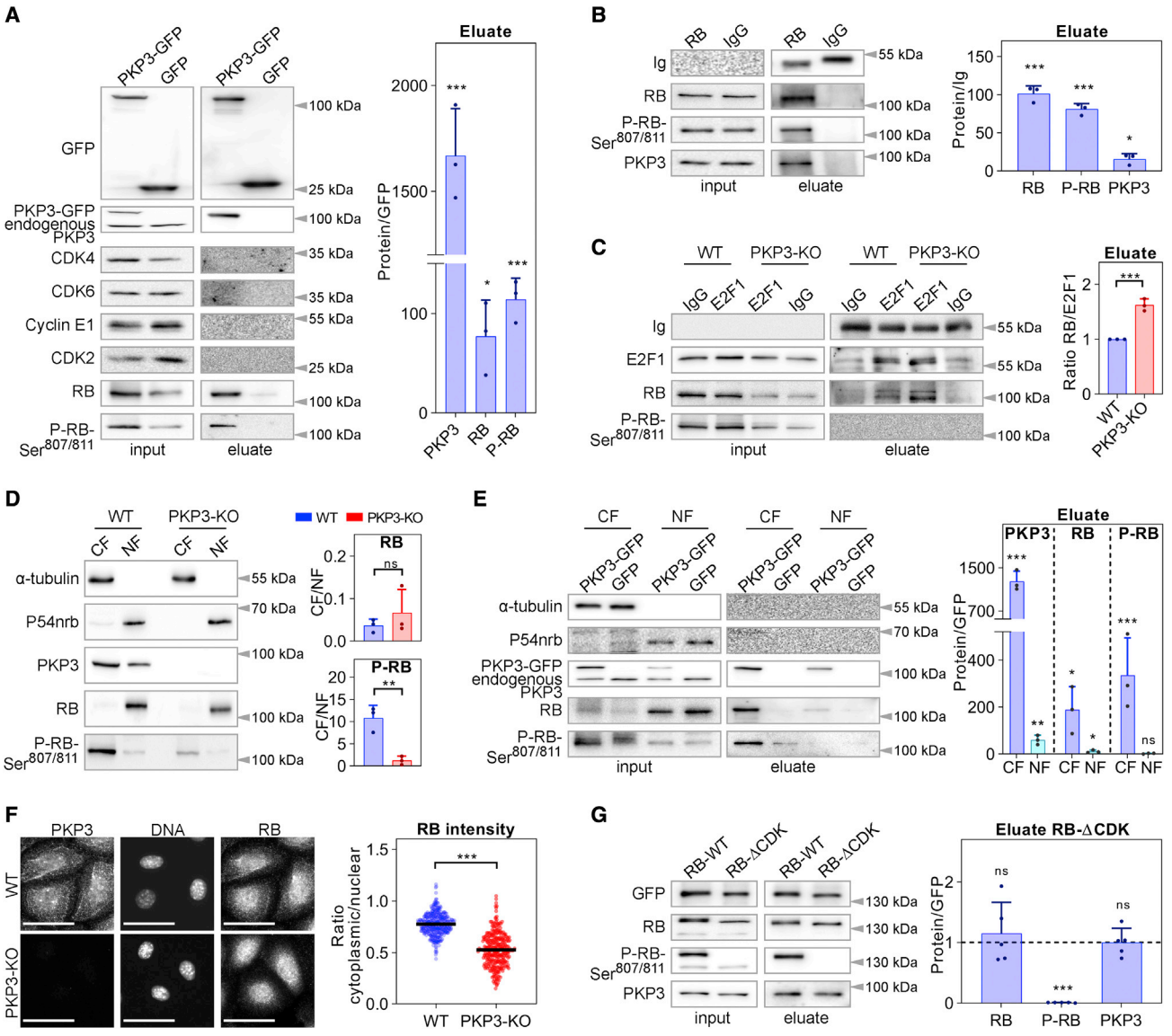

Figure 3. PKP3 captures RB to promote E2F1 release

(A) PKP3-GFP or GFP was affinity purified from WT + GFP or WT + PKP3 cells. Left: representative immunoblot of co-purified proteins. Right: quantification of protein enrichment in PKP3-GFP eluates. Protein concentrations in the eluate were normalized to precipitated GFP and are expressed relative to those of cells expressing GFP alone. Averages + SD from three independent experiments are plotted.

(B) Endogenous RB was affinity purified from WT cells. Left: representative immunoblot of co-purifying proteins. Normal rabbit immunoglobulin G (IgG) served as negative control. Right: quantification of eluate protein levels normalized to IgG heavy chain and relative to values in control cells. Averages + SD from three independent experiments are plotted.

(C) Endogenous E2F1 immunoprecipitation from WT and PKP3-KO cells. Left: representative immunoblots of input and co-purifying proteins. Normal rabbit IgG (Ig) served as a negative control. Right: quantification of the RB/E2F1 protein ratio in the eluate relative to WT cells. Averages + SD from three independent experiments are plotted.

(D) Subcellular fractionation of WT and PKP3-KO cells. Left: representative immunoblot of cytoplasmic fractions (CFs) and nuclear fractions (NFs). Right: quantification of the CF/NF ratio in WT and PKP3-KO cells. Averages + SD from three independent experiments are plotted. For quantification of α-tubulin and P54nrb, see Figure S3.

(E) PKP3-GFP or GFP was affinity purified from ectopically expressing WT cells after subcellular fractionation. Left: representative immunoblot of co-purifying proteins. CF, cytoplasmic fraction; NF, nuclear fraction. Right: protein concentrations in the eluate were normalized to precipitated GFP and are shown relative to those of cells expressing GFP alone Averages + SD from three independent experiments are plotted.

(F) Immunofluorescence analysis of the subcellular localization of RB. Left: representative immunofluorescence images showing RB localization in PKP3-KO and WT cells. Scale bars, 50 μm. Right: cytoplasmic/nuclear ratio of RB fluorescence intensity. n ≥ 300 cells per condition from two independent experiments.

(legend continued on next page)

PKP3 captures RB to promote E2F1 release

To reveal the molecular mechanism underlying the regulation of the G1/S phase transition by PKP3, we analyzed whether PKP3 interacts with proteins involved in the G1/S phase transition. PKP3-GFP was affinity purified from WT + PKP3 cells (Figure 3A). CDK4/CDK6, as well as cyclin E1 and CDK2, did not co-purify with PKP3. In contrast, RB and phospho-RB co-precipitated. The co-purification of PKP3 with endogenous RB immunoprecipitated from WT cells confirmed an association between RB and PKP3 (Figure 3B).

If the interaction of PKP3 with RB facilitates the dissociation of RB from E2F1 the amount of E2F1-RB complex would decrease in the presence of PKP3. To test this assumption, we immunoprecipitated endogenous E2F1 from both WT and PKP3-KO cells (Figure 3C). As expected, phospho-RB did not co-purify with E2F1, whereas RB co-precipitated. However, the amount of the RB-E2F1 complex was significantly higher in PKP3-KO cells, supporting our assumption that PKP3 interferes with their interaction. In conclusion, PKP3 alleviated the RB-E2F1 association, whereas the loss of PKP3 increased the association between E2F1 and RB, leading to reduced E2F1 activity.

As RB phosphorylation during the G1/S phase transition leads to a partial translocation of RB from the nucleus to the cytoplasm, we analyzed its subcellular localization. Subcellular fractionation detected RB in the nucleus of both WT and PKP3-KO cells. In contrast, phospho-RB was primarily detected in the cytoplasm of WT cells, with a strong reduction in PKP3-KO cells (Figure 3D; for validation of cell fractionation see Figure S3). Therefore, we speculated that PKP3 captures phospho-RB in the cytoplasm to promote the G1/S phase transition. To verify this hypothesis, we combined subcellular fractionation with PKP3 immunoprecipitation. Nuclear and cytoplasmic fractions were prepared from WT + PKP3 cells, and PKP3-GFP was affinity purified from both fractions, with the amount in the cytoplasm clearly predominating (Figure 3E). RB co-isolated with PKP3 predominantly in the cytoplasmic fraction, though RB localized primarily in the nucleus. This suggested an association of PKP3 with the phosphorylated form of RB that translocates into the cytoplasm. To further validate the PKP3-dependent localization of RB, WT and PKP3-KO cells were processed for immunofluorescence (Figure 3F). In agreement with the cell fractionation studies, RB predominantly localized in the nucleus with a weaker cytoplasmic signal. Loss of PKP3 further decreased the ratio of cytoplasmic to nuclear RB fluorescence, indicating that PKP3 increased the amount of cytoplasmic RB.

Our findings suggest that PKP3 interacted preferentially with phospho-RB in the cytoplasm. However, these experiments did not allow us to distinguish whether the association depended on RB-phosphorylation or whether it was rather regulated by RB localization. Therefore, we used an RBΔCDK mutant lacking all 15 CDK phosphorylation sites, which were exchanged to alanine (Figure 3G).[16] GFP-tagged WT-RB and RBΔCDK were expressed in WT keratinocytes, and both proteins affinity purified. Using the phospho-RB-Ser807/811 antibody, we confirmed a lack of Ser807/811 phosphorylation in the RBΔCDK mutant. However, PKP3 co-precipitated with RB-WT, as well as RB-ΔCDK, suggesting no preference of PKP3 for phospho- or unphosphorylated RB. Therefore, we conclude that PKP3 does not directly interact with a phosphorylation site in RB. PKP3 either captures phospho-RB after it has been translocated into the cytoplasm or it might facilitate its transport into the cytoplasm.

PKP3 prevents CDKN1A expression to promote RB phosphorylation

The PKP3-phospho-RB interaction can contribute to increased E2F1 activity but does not explain why RB phosphorylation was strongly reduced in PKP3-KO cells. Therefore, we analyzed the regulation of G1/S phase transition upstream of the RB-E2F1 complex in WT and PKP3-KO cells. CDKs are the key enzymes responsible for RB phosphorylation. Their activity is regulated by CDKN proteins. CDKN2A, CDKN2B, and CDKN2D are members of the inhibitors of CDK4 (INK4) family that specifically act on cyclin D-CDK4/CDK6, whereas CDKN1A and CDKN1B are members of the CDK interacting protein/kinase inhibitory protein (CIP/KIP) family that inhibits both cyclin D-CDK4/CDK6 and cyclin E-CDK2 complexes (Figure 4A). Quantification of CDKN transcripts revealed elevated CDKN1A mRNA levels in PKP3-KO cells, whereas CDKN2A mRNA was downregulated (Figure 4B). Accordingly, CDKN1A protein levels were increased in PKP3-KO cells and decreased in WT + PKP3 cells (Figure 4C), whereas CDKN2A protein levels were decreased in PKP3-KO and WT + PKP3 cells. This suggests CDKN1A as the main inhibitory protein with a PKP3-dependent expression pattern.

CDKN1A inhibits proliferation and acts as a tumor suppressor when localized in the nucleus.[17,18] In both WT and PKP3-KO cells, CDKN1A localized predominantly in the nucleus, but the nuclear-to-cytoplasmic ratio of fluorescence intensity was 3-fold higher in PKP3-KO cells than in WT cells (Figure 4D; for validation of antibody specificity, see Figure S4A). As PKP3 interacts with CDKN1A (Figure S4B), we propose that PKP3 sequesters CDKN1A in the cytoplasm to prevent its inhibitory activity. To investigate whether elevated nuclear localization of CDKN1A in PKP3-KO cells resulted in impaired RB phosphorylation, WT and PKP3-KO cells were transfected with control (siCtrl) or CDKN1A-directed (siCDKN1A) small interfering RNAs (siRNAs). Depletion of CDKN1A in PKP3-KO cells diminished CDKN1A protein expression to a level similar to WT cells (Figures 4E and S4C). Importantly, downregulation of CDKN1A in PKP3-KO cells correlated with increased phospho-RB levels (Figure 4E), whereas its ectopic expression in WT cells diminished RB phosphorylation (Figure S4D). The partial rescue of RB phosphorylation after CDKN1A depletion in PKP3-KO cells suggested a critical role of CDKN1A in the PKP3-dependent

(G) GFP-RB-WT or GFP-RBΔCDK was expressed in WT cells and affinity purified. Left: representative immunoblot of co-purifying proteins. Right: quantification of eluate protein levels normalized to precipitated GFP and relative to the values of RB-WT. Averages + SD from five independent experiments are plotted.
*p < 0.05; **p < 0.01; ***p < 0.001; ns, not significant. Significance was determined by Student's unpaired two-tailed t test (A–G) or one-way ANOVA with Tukey's multiple comparisons test (D).

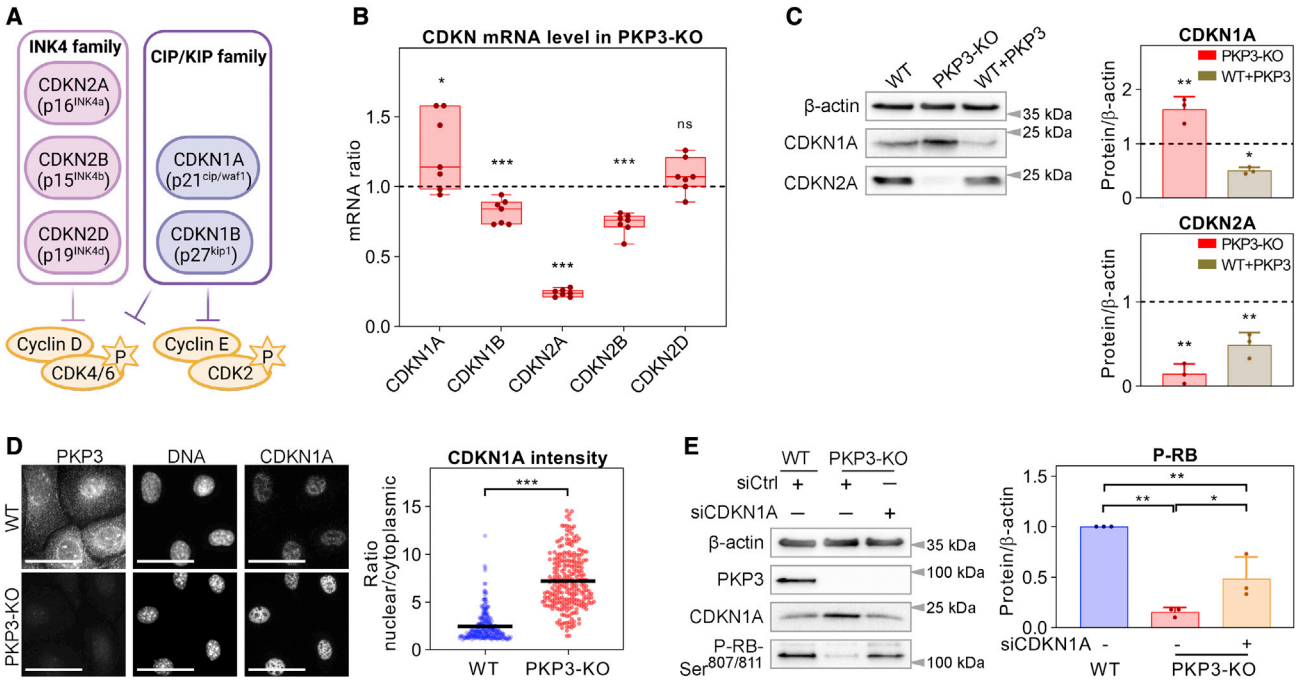

Figure 4. PKP3 prevents CDKN1A expression to promote RB phosphorylation

(A) Schematic of the CDKN gene family. Created with biorender.com.

(B) Amounts of CDKN mRNA in PKP3-KO cells relative to WT cells. *Eif3k* was used as a reference gene. Boxplots show the mRNA ratio from seven independent experiments. The whiskers extend to the minimum and the maximum values.

(C) CDKN1A and CDKN2A protein level. Left: Representative immunoblot of the indicated proteins in WT, PKP3-KO, and WT + PKP3 cells. β-Actin was used as a loading control. Right: quantification of protein levels normalized to β-actin and relative to WT cells. Averages + SD from three independent experiments are plotted.

(D) Immunofluorescence analysis of the subcellular distribution of CDKN1A. Left: representative immunofluorescence images showing CDKN1A localization in WT and PKP3-KO cells. Scale bars, 50 μm. Right: calculated nuclear/cytoplasmic ratio of CDKN1A fluorescence intensity. n ≥ 250 cells per condition from two independent experiments.

(E) Knockdown analysis of CDKN1A in PKP3-KO keratinocytes. Left: representative immunoblot for the indicated proteins in siCtrl and siCDKN1A-transfected WT and PKP3-KO cells. β-Actin was used as the loading control. Right: quantification of phospho-RB levels normalized to β-actin and relative to siCtrl-transfected WT cells. Averages + SD from three independent experiments are plotted.

*p < 0.05; **p < 0.01; ***p < 0.001; ns, not significant. Significance was determined by Student's unpaired two-tailed t test (B and D) or by ANOVA with Tukey's multiple comparisons test (C and E).

See also Figure S4.

regulation of proliferation and confirms an inverse correlation of phospho-RB and CDKN1A levels. We conclude that PKP3 suppresses CDKN1A mRNA and protein expression by a yet-unknown mechanism. By interacting with CDKN1A, PKP3 prevents its nuclear localization to impede its function as an inhibitor of RB phosphorylation.

PKP3 suppresses the RUNX3 transcription factor via an EGFR signaling axis

Elevated CDKN1A mRNA expression in PKP3-KO cells suggested a regulation at the transcriptional level. A number of transcription factors have been reported to regulate CDKN1A expression, including c-MYC[19] and RUNX3, an effector of transforming growth factor β (TGF-β) signaling.[20] Therefore, we investigated whether c-MYC or RUNX3 expression was altered in PKP3-KO cells (Figures 5A and 5B). We analyzed mRNA levels of c-MYC and RUNX3 along with the reference gene *Eif3k* in WT, PKP3-KO, and WT + PKP3 cells (Figure 5B). Though c-MYC mRNA expression was unaltered, RUNX3 Ct values were significantly decreased in PKP3-KO cells and increased in WT + PKP3 cells, indicative of elevated RUNX3 mRNA levels in PKP3-KO cells. Western blotting confirmed unaltered protein levels of c-MYC but dramatically enhanced RUNX3 levels in PKP3-KO cells (Figure 5C), suggesting that elevated RUNX3 may be responsible for elevated CDKN1A and reduced phospho-RB levels in PKP3-KO cells. The depletion of RUNX3 in PKP3-KO cells (Figure S5) reduced the CDKN1A protein amount to a similar level as observed in WT cells (Figure 5D). This confirmed our assumption that RUNX3 regulates CDKN1A expression in murine keratinocytes. Furthermore, phospho-RB was increased in RUNX3-depleted PKP3-KO cells, though it did not reach the level observed in WT cells. The significant, though limited, recovery of RB phosphorylation might be due to the short time frame of the knockdown experiment. However, we cannot rule out that additional processes are involved. For example, PKP3-phospho-RB complex formation might force phospho-RB

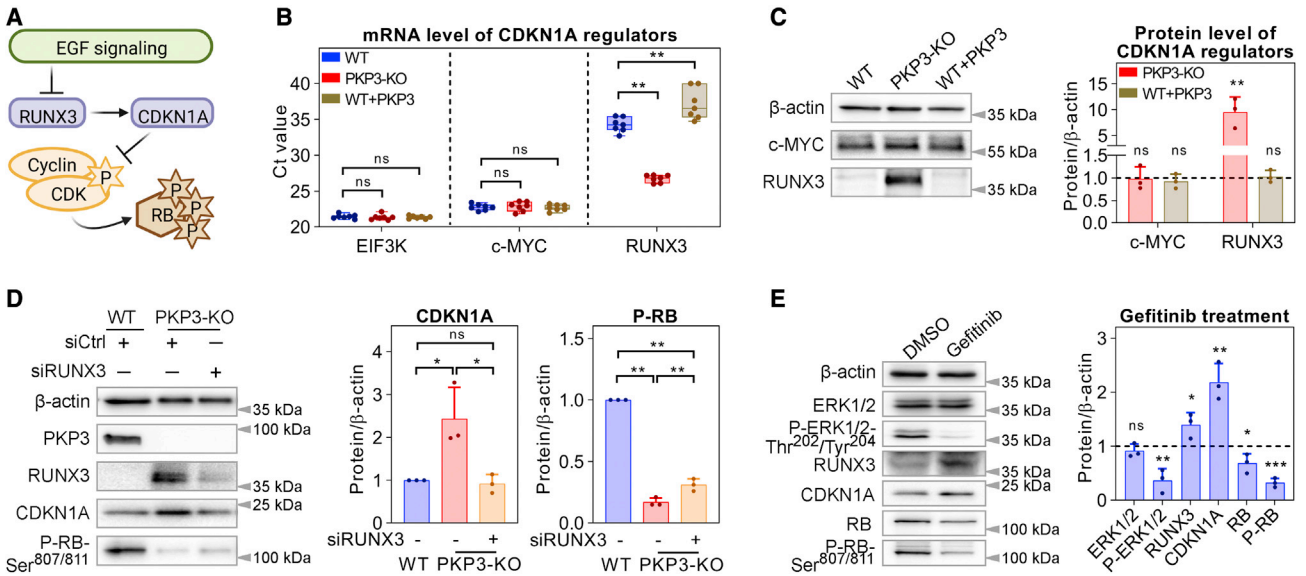

Figure 5. PKP3 suppresses the RUNX3 transcription factor via an EGFR signaling axis

(A) Schematic of the proposed CDKN1A regulation. Created with biorender.com.

(B) Ct values for c-MYC and RUNX3 expressed in WT, PKP3-KO, and WT + PKP3 cells. *Eif3k* was used as a reference gene. Boxplots show Ct values from seven independent qRT-PCR experiments. The whiskers extend to the minimum and the maximum values.

(C) Protein level of c-MYC and RUNX3. Left: representative immunoblot of the indicated proteins in WT, PKP3-KO, and WT + PKP3 cells. β-Actin is shown as the loading control. Right: quantification of protein levels normalized to β-actin and relative to WT cells. Averages + SD from three independent experiments are plotted.

(D) Knockdown analysis of RUNX3. Left: representative immunoblot for the indicated proteins in siCtrl and siRUNX3-transfected WT and PKP3-KO cells. β-Actin was used as a loading control. Right: quantification of protein levels normalized to β-actin and relative to siCtrl-transfected WT cells. Averages + SD from three independent experiments are plotted. See also Figure S5.

(E) EGFR inhibition by gefitinib in WT cells. Left: representative immunoblot of the indicated proteins. DMSO worked as the control treatment and β-actin as the loading control. Right: quantification of protein levels normalized to β-actin and relative to DMSO-treated WT cells. Averages + SD from three independent experiments are plotted.

*p < 0.05; **p < 0.01; ***p < 0.001; ns, not significant. Significance was determined by one-way ANOVA with Tukey's multiple comparisons test (B–D) or by Student's unpaired two-tailed t test (E).

accumulation in WT cells, and PKP3-dependent trapping of CDKN1A in the cytoplasm could also contribute to increased RB phosphorylation in WT cells.

RUNX3 is regulated by TGF-β,[21] and its inactivation is frequently associated with a KRAS-mutated background.[22] We hypothesized that EGF signaling via RAF-RAS-mitogen-activated protein kinases (MAPKs) MEK and ERK controls RUNX3 expression in our non-transformed mouse keratinocytes (Figure 5A). To test this hypothesis, we treated WT cells with gefitinib, a selective EGFR inhibitor (Figure 5E). As expected, gefitinib considerably reduced ERK1/2 phosphorylation. Importantly, RUNX3 and CDKN1A protein levels were increased, suggesting a regulation via the MAPK pathway. Moreover, RB and phospho-RB were decreased in gefitinib-treated WT cells in accordance with enhanced RUNX3 and CDKN1A protein expression. These data indicate that mitogenic signaling via EGF is required to block RUNX3 and CDKN1A expression and allow RB phosphorylation and cell cycle progression.

PKP3 promotes EGFR signaling via a feedback loop

EGFR signaling has been demonstrated to control PKP3 phosphorylation by ribosomal S6 kinase (RSK), thereby modulating PKP3 function in desmosome formation, maturation, and adhesion.[7] Since the inhibition of EGFR signaling mimicked the effects observed in the PKP3-KO cells, we hypothesized that PKP3 might regulate EGFR signaling in a positive feedback loop (Figure 6A). Total EGFR and its phosphorylation at multiple tyrosine residues was decreased in PKP3-KO cells, whereas WT + PKP3 cells had improved EGFR phosphorylation, which correlated with increased activation of its downstream targets MEK1/2, ERK1/2, and RSK. In contrast, RSK phosphorylation was impaired in PKP3-KO cells (Figure 6B). To analyze more directly whether a lack of RSK activity was responsible for the reduced RB phosphorylation, we depleted RSK by RNAi in WT cells. RSK1 knockdown significantly decreased RB phosphorylation, whereas RSK2 depletion did not affect RB expression or phosphorylation (Figure 6C). Thus, RSK1 may be a key driver in RB regulation by PKP3.

As the loss of PKP3 resulted in the dysregulation of EGFR signaling upstream of the RB pathway, we examined whether PKP3 acts as a scaffold to promote EGFR signaling. To identify putative binding partners of PKP3, PKP3-GFP was affinity purified from WT + PKP3 cells and co-isolating proteins detected by immunoblotting (Figure 6D). ERK1/2 and RSK1 co-precipitated, suggesting an interaction between these kinases and PKP3.

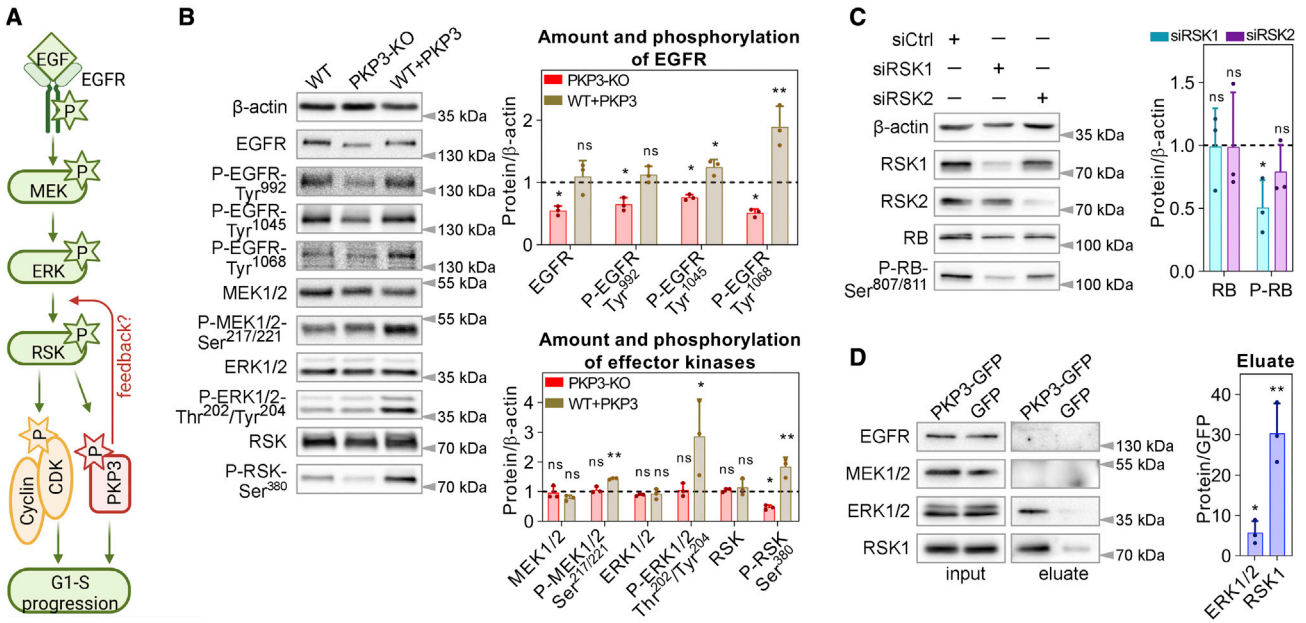

Figure 6. PKP3 promotes EGFR signaling via a feedback loop

(A) Proposed schematic of PKP3 in EGFR signaling and G1/S transition. Created with biorender.com.

(B) Amount and phosphorylation of proteins involved in EGFR signaling. Left: representative immunoblot of the indicated proteins in WT, PKP3-KO, and WT + PKP3 cells. β-Actin was used as the loading control. Right: quantification of protein levels normalized to β-actin and relative to WT cells. Averages + SD from three independent experiments are plotted.

(C) Effect of RSK1 and RSK2 knockdown on RB and phospho-RB levels. Left: representative immunoblot of the indicated proteins in siCtrl, siRSK1, and siRSK2-transfected WT cells. β-Actin was used as the loading control. Right: quantification of protein levels normalized to β-actin and relative to siCtrl-transfected WT cells. Averages + SD from three independent experiments are plotted.

(D) PKP3-GFP or GFP was affinity purified from ectopically expressing WT cells. Left: representative immunoblot of co-purifying proteins. Right: quantification of eluate protein levels normalized to precipitated PKP3-GFP or GFP and relative to values of cells expressing only GFP. Averages + SD from three independent experiments are plotted.

*p < 0.05; **p < 0.01; ***p < 0.001; ns, not significant. Significance was determined by one-way ANOVA with Tukey's multiple comparisons test (B and C) or by Student's unpaired two-tailed t test (D).

Taken together, we propose that PKP3 functions as a scaffold for ERK and RSK to improve RSK1 phosphorylation, thus stimulating signaling downstream of the EGFR.

DISCUSSION

For several desmosomal proteins, a signaling function that allows them to participate in cellular processes, such as proliferation, differentiation, and migration, has been suggested. Disruption of desmosome composition, altered protein expression, or modification can lead to diseases that are accompanied by a deregulation of proliferation and wound healing. PKP3 has not yet been linked to a genetic disease, but PKP3-KO mice were significantly smaller than WT mice, pointing to a role in proliferation.[23] In recent years, many studies have reported elevated PKP3 levels in human cancers, suggesting a role of PKP3 in promoting cancer. Cytoplasmic localization of PKP3 is thought to favor its oncogenic effects.[24] Although such data correlate PKP3 expression with proliferation and cancer, whether and how PKP3 actively promotes proliferation is unclear. Considering the extent of expression differences underlying malignancy, a large number of candidate genes identified based on differential expression do not necessarily drive the cancer phenotype. Additional evidence is necessary to distinguish cancer-driving genes from other alterations.

We used non-transformed keratinocytes to focus on the mechanistic basis of the role of PKP3 in proliferation. We describe a previously unrecognized function of PKP3 as a crucial modulator of proliferation and cell-cycle progression. PKP3 interfered with cell-cycle control at multiple levels; it enhanced mitogenic signaling via the EGFR, leading to increased phosphorylation and activation of RSK. Through this signaling pathway, the expression of the transcription factor RUNX3 and its transcriptional target CDKN1A is inhibited, resulting in the activation of cyclin D-CDK4/6 and cyclin E-CDK2 complexes. This induces phosphorylation of RB and its dissociation from E2F1, which becomes active and initiates the expression of cell-cycle genes. As a result, cells enter S phase. Cell-cycle activation by PKP3 is supported by PKP3 binding to CDKN1A, thereby preventing its inhibitory action in the nucleus. Similarly, PKP3 prevents the inhibitory effect of RB on E2F1 in the nucleus by capturing cytoplasmic RB (summarized in Figure 7). PKP3 appears not to interfere with the onset of the epidermal differentiation program since PKP3-KO cells revealed unaltered or reduced expression of differentiation markers. This indicates that premature differentiation did not

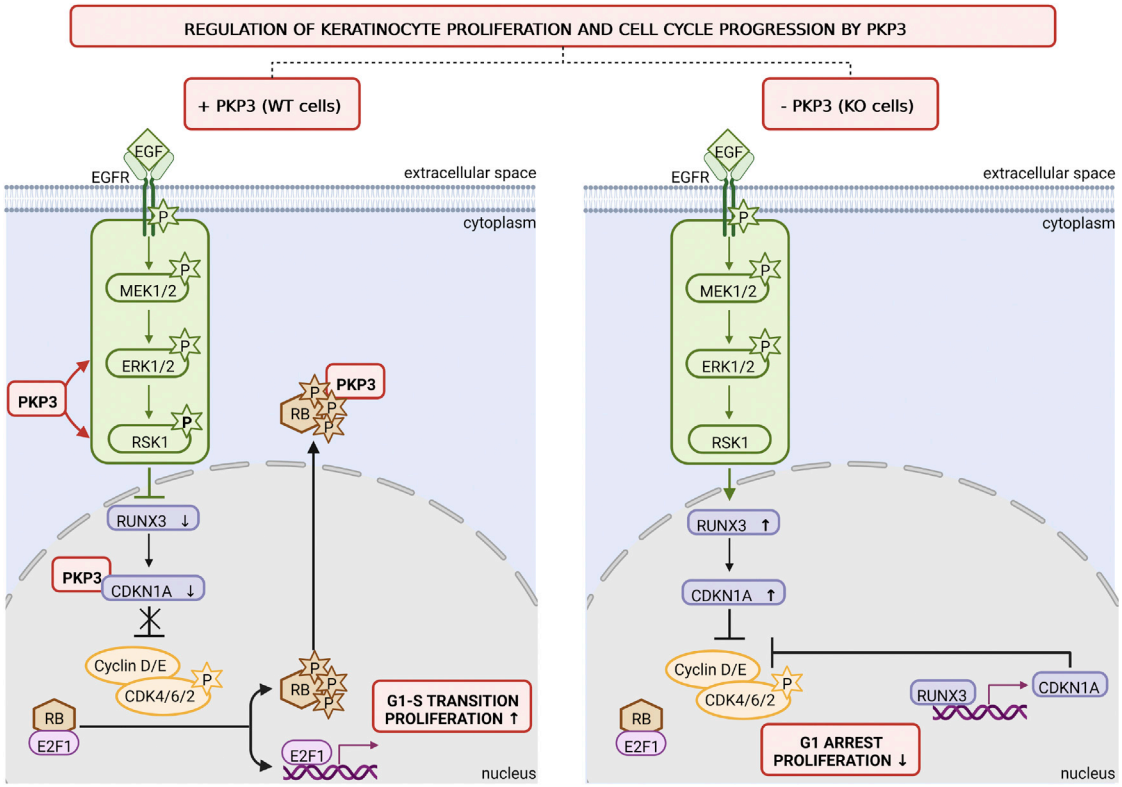

Figure 7. Schematic showing the putative role of PKP3 in the regulation of keratinocyte proliferation

Left: in WT cells, PKP3 promotes EGFR signaling in a positive feedback loop, thereby supporting the downregulation of RUNX3 and its transcriptional target CDKN1A. This promotes the activation of cyclin-CDK complexes, RB phosphorylation, and E2F1 release. PKP3 also sequesters phospho-RB in the cytoplasm to promote E2F1 activity, resulting in the G1/S transition and enhanced proliferation. Right: the loss of PKP3 results in impaired RSK1 phosphorylation, which improves RUNX3 and CDKN1A expression. Elevated nuclear CDKN1A prevents RB phosphorylation and E2F1 target gene expression, leading to G1 arrest and reduced proliferation. Schematic created with biorender.com.

induce a cell-cycle exit of PKP3-KO cells but that these cells rather accumulated in G1 phase.

PKP3 captures RB to promote E2F activity

As phospho-RB was significantly downregulated in PKP3-KO and upregulated in WT + PKP3 cells, we analyzed the PKP3-dependent regulation of RB. CDK-mediated phosphorylation of RB occurs at up to 15 sites and drives structural changes in RB that lead to E2F dissociation.[25] Cyclin D-CDK4/6 mono-phosphorylates RB without an obvious preference for a specific site. Subsequently, cyclin E-CDK2 completes RB phosphorylation to release and fully activate E2F.[26] Although CDK6 expression was reduced in the PKP3-KO cells, its overexpression did not increase RB phosphorylation, suggesting that a lack of CDK6 is not the major driver of prolonged cell-cycle exit.

Using immunoprecipitation, we demonstrate an association between PKP3 and phospho-RB. Cell fractionation and immunofluorescence studies suggested that the interaction occurred primarily in the cytoplasm, though the majority of total RB localized in the nucleus. This implies that PKP3 interacts primarily with phospho-RB *in vivo*, as only phospho-RB localizes in the cytoplasm. However, phosphorylation was not a prerequisite for PKP3 binding. An RB mutant lacking all CDK phosphorylation sites[16] was still able to bind PKP3, indicating that these sites are not identical with the PKP3 binding site. Mechanistically this means that the interaction is regulated by intracellular localization, which depends on RB phosphorylation, and that PKP3 binds and retains phospho-RB in the cytoplasm, thereby preventing its de-phosphorylation and/or inhibitory function in the nucleus to improve E2F activity and promote proliferation.

Although the majority of RB localizes in the nucleus, a cytoplasmic localization has been observed before. A recent study identified cytoplasmic RB-interacting proteins.[27] PKP3 was not detected in this study, perhaps because of a lack of expression in the cell line used. However, related proteins from adherens junctions such as β-catenin and δ-catenin were identified as putative RB-interacting proteins. These proteins revealed a preference for binding to WT compared with RBΔCDK mutants, suggesting that they may preferentially interact with phospho-RB. However, the relevance of this finding and the molecular mechanisms require further investigation.

PKP3 controls an EGF-RSK-RUNX3-CDKN1A axis to promote cell proliferation

Another important event at the G1/S transition is the degradation of CDKN1A/CDKN1B, which is required for RB inactivation.[28,29]

CDKN1A not only influences proliferation via protein-protein interactions with cyclins and/or CDKs but can also interact directly with E2F1, reducing its transcriptional activity.[30] Nuclear CDKN1A inactivates the cyclin-CDK complexes to prevent cell-cycle progression, thus acting as a tumor suppressor.[17] Elevated nuclear CDKN1A levels in PKP3-KO point to a central role of CDKN1A in G0/G1 arrest in these cells. CDKN1A expression in PKP3-KO cells correlated with increased expression of the tumor suppressor RUNX3. Deletion of *RUNX3* in mouse lung caused the development of lung adenomas and accelerated K-Ras-induced progression into adenocarcinomas.[22] We confirmed the positive correlation between RUNX3 and CDKN1A expression and show that EGFR signaling suppresses RUNX3 and CDKN1A.

Stem cells reside in the basal layer of the epidermis, where they self-renew or generate committed cells that undergo terminal differentiation. EGFR signaling maintains keratinocytes in the basal layer of the epidermis in a proliferative state, and the maintenance of epidermal stem cells depends on ERK activity.[31] Deregulation of EGFR signaling either by overexpression or by activating mutations in the receptor is frequently observed in tumors, and some data point to a putative role of PKP3 in this pathway,[4] although the molecular mechanisms underlying PKP3-mediated modulation of EGFR signaling are unknown. A BioID (proximity-dependent biotin identification) approach to identify EGFR-specific binding partners identified PKP3 in close proximity to the EGFR, but the association did not correlate with a specific EGFR-mutant state.[32] In our hands, EGFR did not co-purify with PKP3 from mouse keratinocytes. This finding is in agreement with another study that analyzed interactions between overexpressed PKPs and EGFR.[33] We expect that differences in the experimental settings are responsible for the discrepancy, the most important of which is that BioID relies on proximity labeling and does not depend on a stable complex that persists during affinity purification. Therefore, we may have missed a rather transient interaction. On the other hand, BioID may identify proteins that localize in proximity to the bait protein without a functional link.

Other studies support a link between PKP3 and mitogenic signaling downstream of EGFR. In ovarian cancer cells, PKP3 silencing correlates with decreased phosphorylation of ERK1/2, whereas PKP3 overexpression increases ERK1/2 phosphorylation and cell proliferation.[34] PKP3 itself is regulated by RSK downstream of ERK in the EGFR pathway.[7] Multiple RSK substrates are involved in the regulation of proliferation.[35] Here, we confirmed a role of RSK1 in RB phosphorylation and show that loss of PKP3 decreased RSK phosphorylation. RSK1 activation is initiated by an interaction with ERK[36] that induces RSK1 auto-phosphorylation at Ser380. Subsequent full activation allows RSKs to phosphorylate downstream targets, including PKP3. PKP3 interacts with both ERK1/2 and RSK1, raising the possibility that it acts as a scaffold for the two kinases to extend signaling downstream of the EGFR.

Role of PKP3 in cancer

As we uncovered a role of PKP3 in promoting cell-cycle progression and proliferation, we wondered how this correlates with the putative role of PKP3 in cancer. A recent study investigated PKP3 expression in different tumor types using public datasets[37] and revealed enhanced PKP3 expression in tumor tissue from breast cancer, colon cancer, clear cell renal cell carcinoma, lung adenocarcinoma, uterine corpus endometrial carcinoma, and ovarian carcinoma compared with normal tissue. Elevated expression of PKP3 has also been described in the majority of cases of non-small cell lung cancer,[11] ovarian cancer,[38] breast cancer,[39] and prostate adenocarcinoma.[10] In non-small cell lung carcinoma, increased PKP3 expression correlated with poor prognosis and reduced survival. In these cells, PKP3 knockdown reduced cell growth,[11] as we observe in our PKP3-KO keratinocytes. Our findings support a role of PKP3 as an oncogene facilitating tumor cell growth. However, some cancer-driving genes can exhibit oncogene or tumor-suppressor behavior depending on the biological context, and such genes were designated "dual-role cancer driver genes."[40] We think that PKP3 is one of these dual-role cancer driver proteins because its role may depend on tissue and cell type and on the activation of specific signaling pathways. Downregulation has been observed, for example, in bladder cancer.[41] Knocking down PKP3 in HCT116 cells revealed accelerated tumor formation in nude mice and increased metastasis to the lungs, suggesting that PKP3 may be lost in invasive and metastatic tumors.[42]

Despite distinct functions in adhesion and signaling, the basic principle that intracellular localization determines function is conserved between PKP1 and PKP3. PKP1 acts as a tumor suppressor in desmosomes or as an oncogene in the cytoplasm, where it stimulates proliferation by enhancing protein synthesis in an eIF4A-dependent pathway.[43] This is controlled by AKT2 signaling.[44] Activated AKT2 is commonly observed in squamous cell carcinoma, and cutaneous human papillomaviruses (HPVs) may support focal AKT2 activation in skin tumorigenesis.[45] Thus, it may be a general principle that PKPs are dual-role cancer driver genes with tumor-suppressive characteristics when localized in desmosomes and oncogenic features in the cytoplasm or nucleus.

Limitations of the study

Although this study considerably advances our understanding of the role of PKP3 in regulating proliferation, several questions remain to be addressed. PKP3 regulates cell-cycle progression and proliferation via an ERK-RSK-CDKN1A-RB signaling axis. However, the contribution of each individual interaction with ERK/RSK, CDKN1A, or RB remains to be characterized in detail.

Another limitation is that the canonical G1/S pathway is currently understood as being linear, with the cyclin-CDK complexes inactivating RB, thereby allowing the E2F to promote the transcription of cell-cycle-related genes, but regulation *in vivo* is much more complex. Multiple homologous proteins, post-translational modifications, and positive and negative feedback loops modulate and connect the different pathway components.

Conflicting roles have been reported for CDKN1A in cancer, classifying CDKN1A as another dual-role cancer driving gene. The cell-cycle regulatory roles of CDKN1A seem to depend on its expression level, with low levels promoting cyclin D-CDK4/6 activation and high levels mediating cyclin-CDK inhibition. Moreover, the inhibitory function depends on its nuclear localization, whereas a cytoplasmic pool determines a survival function.[46]

Therefore, a detailed characterization of PKP3's role in the regulation of CDKN1A expression and localization may advance our understanding of its role in growth control.

Finally, it remains to be determined if and how PKP3 promotes cell proliferation in cancer cells. The E2F1-RB axis is altered in most cancers, and the tumor suppressor RB is frequently inactivated. Such mutations in the RB/E2F1 axis facilitate aberrant cell proliferation.[47] Further studies are required to investigate how PKP3 promotes proliferation in cells with deregulated RB/E2F1 activity and how its role in proliferation correlates with aberrant EGFR pathway activation.

STAR★METHODS

Detailed methods are provided in the online version of this paper and include the following:

- KEY RESOURCES TABLE
- RESOURCE AVAILABILITY
  - Lead contact
  - Materials availability
  - Data and code availability
- EXPERIMENTAL MODEL AND SUBJECT DETAILS
  - Cell lines, cell culture and treatments
  - Transfections
  - Plasmids and cloning
- METHODS DETAILS
  - Cell proliferation assay
  - Cell cycle analyses
  - BrdU assay
  - Protein extraction
  - Nucleus/cytoplasm fractionation
  - Immunoprecipitation
  - Validation of P-RB-Ser807/811 antibody
  - SDS-PAGE and immunoblotting
  - RNA expression
  - Immunofluorescence analysis and image processing
- QUANTIFICATION AND STATISTICAL ANALYSIS
  - Immunoblot quantification
  - Quantification of immunofluorescence
  - Statistical analysis

SUPPLEMENTAL INFORMATION

Supplemental information can be found online at https://doi.org/10.1016/j.celrep.2023.112031.

ACKNOWLEDGMENTS

We thank Andrej Mun for technical assistance and Dr. Nadine Bley from the Core Facility Imaging (CFI) at the Martin Luther University Halle for competent support with InCucyte proliferation analyses. This work was supported by the German Research Council (DFG) SPP1782, grants Ha-1791/10-1 and Ha1791/10-2 to M.H. We acknowledge the financial support of the Open Access Publication Fund of the Martin Luther University Halle.

AUTHOR CONTRIBUTIONS

Conceptualization, L.M. and M.H.; funding acquisition, M.H.; experiments, L.M. and R.K.; writing, L.M. and M.H.; editing, L.M., R.K., and M.H.

DECLARATION OF INTERESTS

The authors declare no competing interests.

Received: June 2, 2022
Revised: October 26, 2022
Accepted: January 10, 2023

REFERENCES

1. Perez-Moreno, M., and Fuchs, E. (2006). Catenins: keeping cells from getting their signals crossed. Dev. Cell *11*, 601–612. https://doi.org/10.1016/j.devcel.2006.10.010.
2. Rübsam, M., Broussard, J.A., Wickström, S.A., Nekrasova, O., Green, K.J., and Niessen, C.M. (2018). Adherens junctions and desmosomes coordinate mechanics and signaling to orchestrate tissue morphogenesis and function: an evolutionary perspective. Cold Spring Harb. Perspect. Biol. *10*, a029207. https://doi.org/10.1101/cshperspect.a029207.
3. Green, K.J., and Simpson, C.L. (2007). Desmosomes: new perspectives on a classic. J. Invest. Dermatol. *127*, 2499–2515. https://doi.org/10.1038/sj.jid.5701015.
4. Müller, L., Hatzfeld, M., and Keil, R. (2021). Desmosomes as signaling hubs in the regulation of cell behavior. Front. Cell Dev. Biol. *9*, 745670. https://doi.org/10.3389/fcell.2021.745670.
5. Bass-Zubek, A.E., Godsel, L.M., Delmar, M., and Green, K.J. (2009). Plakophilins: multifunctional scaffolds for adhesion and signaling. Curr. Opin. Cell Biol. *21*, 708–716. https://doi.org/10.1016/j.ceb.2009.07.002.
6. Hatzfeld, M., Wolf, A., and Keil, R. (2014). Plakophilins in desmosomal adhesion and signaling. Cell Commun. Adhes. *21*, 25–42. https://doi.org/10.3109/15419061.2013.876017.
7. Müller, L., Rietscher, K., Keil, R., Neuholz, M., and Hatzfeld, M. (2020). Plakophilin 3 phosphorylation by ribosomal S6 kinases supports desmosome assembly. J. Cell Sci. *133*, jcs238295. https://doi.org/10.1242/jcs.238295.
8. Hofmann, I., Casella, M., Schnölzer, M., Schlechter, T., Spring, H., and Franke, W.W. (2006). Identification of the junctional plaque protein plakophilin 3 in cytoplasmic particles containing RNA-binding proteins and the recruitment of plakophilins 1 and 3 to stress granules. Mol. Biol. Cell *17*, 1388–1398. https://doi.org/10.1091/mbc.e05-08-0708.
9. Roberts, B.J., Reddy, R., and Wahl, J.K., 3rd. (2013). Stratifin (14-3-3 sigma) limits plakophilin-3 exchange with the desmosomal plaque. PLoS One *8*, e77012. https://doi.org/10.1371/journal.pone.0077012.
10. Breuninger, S., Reidenbach, S., Sauer, C.G., Ströbel, P., Pfitzenmaier, J., Trojan, L., and Hofmann, I. (2010). Desmosomal plakophilins in the prostate and prostatic adenocarcinomas: implications for diagnosis and tumor progression. Am. J. Pathol. *176*, 2509–2519. https://doi.org/10.2353/ajpath.2010.090737.
11. Furukawa, C., Daigo, Y., Ishikawa, N., Kato, T., Ito, T., Tsuchiya, E., Sone, S., and Nakamura, Y. (2005). Plakophilin 3 oncogene as prognostic marker and therapeutic target for lung cancer. Cancer Res. *65*, 7102–7110. https://doi.org/10.1158/0008-5472.CAN-04-1877.
12. Valladares-Ayerbes, M., Díaz-Prado, S., Reboredo, M., Medina, V., Lorenzo-Patiño, M.J., Iglesias-Díaz, P., Haz, M., Pértega, S., Santamarina, I., Blanco, M., et al. (2010). Evaluation of plakophilin-3 mRNA as a biomarker for detection of circulating tumor cells in gastrointestinal cancer patients. Cancer Epidemiol. Biomarkers Prev. *19*, 1432–1440. https://doi.org/10.1158/1055-9965.EPI-10-0123.
13. Gao, L., Li, X., Guo, Q., Nie, X., Hao, Y., Liu, Q., Liu, J., Zhu, L., Yan, L., and Lin, B. (2020). Identification of PKP 2/3 as potential biomarkers of ovarian cancer based on bioinformatics and experiments. Cancer Cell Int. *20*, 509. https://doi.org/10.1186/s12935-020-01602-3.
14. Keil, R., Rietscher, K., and Hatzfeld, M. (2016). Antagonistic regulation of intercellular cohesion by plakophilins 1 and 3. J. Invest. Dermatol. *136*, 2022–2029. https://doi.org/10.1016/j.jid.2016.05.124.

15. Cho, I.J., Lui, P.P., Obajdin, J., Riccio, F., Stroukov, W., Willis, T.L., Spagnoli, F., and Watt, F.M. (2019). Mechanisms, hallmarks, and implications of stem cell quiescence. Stem Cell Rep. *12*, 1190–1200. https://doi.org/10.1016/j.stemcr.2019.05.012.

16. Narasimha, A.M., Kaulich, M., Shapiro, G.S., Choi, Y.J., Sicinski, P., and Dowdy, S.F. (2014). Cyclin D activates the Rb tumor suppressor by mono-phosphorylation. Elife *3*, e02872. https://doi.org/10.7554/eLife.02872.

17. Al Bitar, S., and Gali-Muhtasib, H. (2019). The role of the cyclin dependent kinase inhibitor p21(cip1/waf1) in targeting cancer: molecular mechanisms and novel therapeutics. Cancers *11*, 1475. https://doi.org/10.3390/cancers11101475.

18. Georgakilas, A.G., Martin, O.A., and Bonner, W.M. (2017). p21: a two-faced genome guardian. Trends Mol. Med. *23*, 310–319. https://doi.org/10.1016/j.molmed.2017.02.001.

19. Abbas, T., and Dutta, A. (2009). p21 in cancer: intricate networks and multiple activities. Nat. Rev. Cancer *9*, 400–414. https://doi.org/10.1038/nrc2657.

20. Chi, X.Z., Yang, J.O., Lee, K.Y., Ito, K., Sakakura, C., Li, Q.L., Kim, H.R., Cha, E.J., Lee, Y.H., Kaneda, A., et al. (2005). RUNX3 suppresses gastric epithelial cell growth by inducing p21(WAF1/Cip1) expression in cooperation with transforming growth factor {beta}-activated SMAD. Mol. Cell Biol. *25*, 8097–8107. https://doi.org/10.1128/MCB.25.18.8097-8107.2005.

21. Ito, Y., and Miyazono, K. (2003). RUNX transcription factors as key targets of TGF-beta superfamily signaling. Curr. Opin. Genet. Dev. *13*, 43–47. https://doi.org/10.1016/s0959-437x(03)00007-8.

22. Lee, Y.S., Lee, J.W., Jang, J.W., Chi, X.Z., Kim, J.H., Li, Y.H., Kim, M.K., Kim, D.M., Choi, B.S., Kim, E.G., et al. (2013). Runx3 inactivation is a crucial early event in the development of lung adenocarcinoma. Cancer Cell *24*, 603–616. https://doi.org/10.1016/j.ccr.2013.10.003.

23. Sklyarova, T., Bonné, S., D'Hooge, P., Denecker, G., Goossens, S., De Rycke, R., Borgonie, G., Bösl, M., van Roy, F., and van Hengel, J. (2008). Plakophilin-3-deficient mice develop hair coat abnormalities and are prone to cutaneous inflammation. J. Invest. Dermatol. *128*, 1375–1385. https://doi.org/10.1038/sj.jid.5701189.

24. Dusek, R.L., and Attardi, L.D. (2011). Desmosomes: new perpetrators in tumour suppression. Nat. Rev. Cancer *11*, 317–323. https://doi.org/10.1038/nrc3051.

25. Dick, F.A., and Rubin, S.M. (2013). Molecular mechanisms underlying RB protein function. Nat. Rev. Mol. Cell Biol. *14*, 297–306. https://doi.org/10.1038/nrm3567.

26. Rubin, S.M., Sage, J., and Skotheim, J.M. (2020). Integrating old and new paradigms of G1/S control. Mol. Cell *80*, 183–192. https://doi.org/10.1016/j.molcel.2020.08.020.

27. Sanidas, I., Morris, R., Fella, K.A., Rumde, P.H., Boukhali, M., Tai, E.C., Ting, D.T., Lawrence, M.S., Haas, W., and Dyson, N.J. (2019). A code of mono-phosphorylation modulates the function of RB. Mol. Cell *73*, 985–1000.e6. https://doi.org/10.1016/j.molcel.2019.01.004.

28. Barr, A.R., Heldt, F.S., Zhang, T., Bakal, C., and Novák, B. (2016). A dynamical framework for the all-or-none G1/S transition. Cell Syst. *2*, 27–37. https://doi.org/10.1016/j.cels.2016.01.001.

29. Heldt, F.S., Barr, A.R., Cooper, S., Bakal, C., and Novák, B. (2018). A comprehensive model for the proliferation-quiescence decision in response to endogenous DNA damage in human cells. Proc. Natl. Acad. Sci. USA *115*, 2532–2537. https://doi.org/10.1073/pnas.1715345115.

30. Radhakrishnan, S.K., Feliciano, C.S., Najmabadi, F., Haegebarth, A., Kandel, E.S., Tyner, A.L., and Gartel, A.L. (2004). Constitutive expression of E2F-1 leads to p21-dependent cell cycle arrest in S phase of the cell cycle. Oncogene *23*, 4173–4176. https://doi.org/10.1038/sj.onc.1207571.

31. Hiratsuka, T., Bordeu, I., Pruessner, G., and Watt, F.M. (2020). Regulation of ERK basal and pulsatile activity control proliferation and exit from the stem cell compartment in mammalian epidermis. Proc. Natl. Acad. Sci. USA *117*, 17796–17807. https://doi.org/10.1073/pnas.2006965117.

32. Erdem-Eraslan, L., Gao, Y., Kloosterhof, N.K., Atlasi, Y., Demmers, J., Sacchetti, A., Kros, J.M., Sillevis Smitt, P., Aerts, J., and French, P.J. (2015). Mutation specific functions of EGFR result in a mutation-specific downstream pathway activation. Eur. J. Cancer *51*, 893–903. https://doi.org/10.1016/j.ejca.2015.02.006.

33. Arimoto, K.i., Burkart, C., Yan, M., Ran, D., Weng, S., and Zhang, D.E. (2014). Plakophilin-2 promotes tumor development by enhancing ligand-dependent and -independent epidermal growth factor receptor dimerization and activation. Mol. Cell Biol. *34*, 3843–3854. https://doi.org/10.1128/MCB.00758-14.

34. Lim, V., Zhu, H., Diao, S., Hu, L., and Hu, J. (2019). PKP3 interactions with MAPK-JNK-ERK1/2-mTOR pathway regulates autophagy and invasion in ovarian cancer. Biochem. Biophys. Res. Commun. *508*, 646–653. https://doi.org/10.1016/j.bbrc.2018.11.163.

35. Anjum, R., and Blenis, J. (2008). The RSK family of kinases: emerging roles in cellular signalling. Nat. Rev. Mol. Cell Biol. *9*, 747–758. https://doi.org/10.1038/nrm2509.

36. Smith, J.A., Poteet-Smith, C.E., Malarkey, K., and Sturgill, T.W. (1999). Identification of an extracellular signal-regulated kinase (ERK) docking site in ribosomal S6 kinase, a sequence critical for activation by ERK in vivo. J. Biol. Chem. *274*, 2893–2898. https://doi.org/10.1074/jbc.274.5.2893.

37. Ruan, S., Shi, J., Wang, M., and Zhu, Z. (2021). Analysis of multiple human tumor cases reveals the carcinogenic effects of PKP3. J. Healthc. Eng. *2021*, 9391104. https://doi.org/10.1155/2021/9391104.

38. Qian, H., Yuan, D., Bao, J., Liu, F., Zhang, W., Yang, X., Han, G., Huang, J., Sheng, H., and Yu, H. (2019). Increased expression of plakophilin 3 is associated with poor prognosis in ovarian cancer. Medicine *98*, e14608. https://doi.org/10.1097/MD.0000000000014608.

39. Demirag, G.G., Sullu, Y., and Yucel, I. (2012). Expression of Plakophilins (PKP1, PKP2, and PKP3) in breast cancers. Med. Oncol. *29*, 1518–1522. https://doi.org/10.1007/s12032-011-0071-1.

40. Colaprico, A., Olsen, C., Bailey, M.H., Odom, G.J., Terkelsen, T., Silva, T.C., Olsen, A.V., Cantini, L., Zinovyev, A., Barillot, E., et al. (2020). Interpreting pathways to discover cancer driver genes with Moonlight. Nat. Commun. *11*, 69. https://doi.org/10.1038/s41467-019-13803-0.

41. Takahashi, H., Nakatsuji, H., Takahashi, M., Avirmed, S., Fukawa, T., Takemura, M., Fukumori, T., and Kanayama, H. (2012). Up-regulation of plakophilin-2 and Down-regulation of plakophilin-3 are correlated with invasiveness in bladder cancer. Urology *79*, 240.e1-e8. https://doi.org/10.1016/j.urology.2011.08.049.

42. Kundu, S.T., Gosavi, P., Khapare, N., Patel, R., Hosing, A.S., Maru, G.B., Ingle, A., Decaprio, J.A., and Dalal, S.N. (2008). Plakophilin3 downregulation leads to a decrease in cell adhesion and promotes metastasis. Int. J. Cancer *123*, 2303–2314. https://doi.org/10.1002/ijc.23797.

43. Wolf, A., Krause-Gruszczynska, M., Birkenmeier, O., Ostareck-Lederer, A., Hüttelmaier, S., and Hatzfeld, M. (2010). Plakophilin 1 stimulates translation by promoting eIF4A1 activity. J. Cell Biol. *188*, 463–471. https://doi.org/10.1083/jcb.200908135.

44. Wolf, A., Rietscher, K., Glaß, M., Hüttelmaier, S., Schutkowski, M., Ihling, C., Sinz, A., Wingenfeld, A., Mun, A., and Hatzfeld, M. (2013). Insulin signaling via Akt2 switches plakophilin 1 function from stabilizing cell adhesion to promoting cell proliferation. J. Cell Sci. *126*, 1832–1844. https://doi.org/10.1242/jcs.118992.

45. O'Shaughnessy, R.F.L., Akgül, B., Storey, A., Pfister, H., Harwood, C.A., and Byrne, C. (2007). Cutaneous human papillomaviruses down-regulate AKT1, whereas AKT2 up-regulation and activation associates with tumors. Cancer Res. *67*, 8207–8215. https://doi.org/10.1158/0008-5472.CAN-07-0755.

46. Jung, Y.S., Qian, Y., and Chen, X. (2010). Examination of the expanding pathways for the regulation of p21 expression and activity. Cell. Signal. *22*, 1003–1012. https://doi.org/10.1016/j.cellsig.2010.01.013.

47. Fouad, S., Hauton, D., and D'Angiolella, V. (2020). E2F1: cause and consequence of DNA replication stress. Front. Mol. Biosci. *7*, 599332. https://doi.org/10.3389/fmolb.2020.599332.

48. van den Heuvel, S., and Harlow, E. (1993). Distinct roles for cyclin-dependent kinases in cell cycle control. Science *262*, 2050–2054. https://doi.org/10.1126/science.8266103.

49. Zhou, B.P., Liao, Y., Xia, W., Spohn, B., Lee, M.H., and Hung, M.C. (2001). Cytoplasmic localization of p21Cip1/WAF1 by Akt-induced phosphorylation in HER-2/neu-overexpressing cells. Nat. Cell Biol. *3*, 245–252. https://doi.org/10.1038/35060032.

50. Schindelin, J., Arganda-Carreras, I., Frise, E., Kaynig, V., Longair, M., Pietzsch, T., Preibisch, S., Rueden, C., Saalfeld, S., Schmid, B., et al. (2012). Fiji: an open-source platform for biological-image analysis. Nat. Methods *9*, 676–682. https://doi.org/10.1038/nmeth.2019.

STAR★METHODS

KEY RESOURCES TABLE

REAGENT or RESOURCE	SOURCE	IDENTIFIER
Antibodies		
CDK2 rabbit monoclonal antibody	Cell Signaling Technology	Cat# 2546S; RRID: AB_2276129
CDK4 mouse monoclonal antibody	Santa Cruz Biotechnology	Cat# sc-23896; RRID: AB_627239
CDK6 mouse monoclonal antibody	Cell Signaling Technology	Cat# 3136S; RRID: AB_2229289
CDKN1A rabbit polyclonal antibody	Cell Signaling Technology	Cat# 64016S; RRID: AB_2892063
CDKN2A rabbit polyclonal antibody	Thermo Fisher Scientific	Cat# PA1-30670; RRID: AB_1956784
c-Myc rabbit monoclonal antibody	Cell Signaling Technology	Cat# 5605S; RRID: AB_1903938
Corneodesmosin (CSDN) rabbit polyclonal antibody	Sigma-Aldrich	Cat# HPA044730; RRID: AB_10964923
Cyclin D1 rabbit monoclonal antibody	Cell Signaling Technology	Cat# 2978S; RRID: AB_2259616
Cyclin D2 rabbit monoclonal antibody	Cell Signaling Technology	Cat# 3741S; RRID: AB_2070685
Cyclin E1 rabbit monoclonal antibody	Cell Signaling Technology	Cat# 20808S; RRID: AB_2783554
Desmoglein1 (DSG1) mouse monoclonal antibody	Progen	Cat# 61002; RRID: AB_2891034
E2F1 rabbit polyclonal antibody	Abcam	Cat# ab137415
EGFR rabbit monoclonal antibody	Cell Signaling Technology	Cat# 4267; RRID: AB_2864406
ERK1/2 mouse monoclonal antibody	Cell Signaling Technology	Cat# 9102; RRID: AB_330744
GFP rabbit polyclonal antibody	Rockland	Cat# 600-401-215; RRID: AB_828167
Involucrin mouse monoclonal antibody	Santa Cruz Biotechnology	Cat# sc-21748; RRID: AB_2128119
Keratin 1 rabbit polyclonal customized peptide specific antibody	Peptide Specialty Laboratories	N/A
Keratin 10 rabbit polyclonal customized peptide specific antibody	Peptide Specialty Laboratories	N/A
Loricrin rabbit polyclonal antibody	GeneTex	Cat# GTX116013; RRID: AB_2037360
MEK1/2 mouse monoclonal antibody	Cell Signaling Technology	Cat# 4694; RRID: AB_10695868
P54 (nrb) mouse monoclonal antibody	BD Transduction Laboratories	Cat# 611279; RRID: AB_398807
Phospho-CDK2 (Thr160) rabbit polyclonal antibody	Cell Signaling Technology	Cat# 2561; RRID: AB_2078685
Phospho-CDK4 (Thr172) rabbit polyclonal antibody	Thermo Fisher Scientific	Cat# PA5-64482; RRID: AB_2662543
Phospho-CDK6 (Tyr24) rabbit polyclonal antibody	Thermo Fisher Scientific	Cat# PA5-104683; RRID: AB_2816158
Phospho-CDK6 (Thr177) rabbit recombinant polyclonal antibody	Thermo Fisher Scientific	Cat# 711588; RRID: AB_2632988
Phospho-EGFR (Tyr992) rabbit polyclonal antibody	Cell Signaling Technology	Cat# 2235S; RRID: AB_331708
Phospho-EGFR (Tyr1045) rabbit polyclonal antibody	Cell Signaling Technology	Cat# 2237S
Phospho-EGFR (Tyr1068) rabbit monoclonal antibody	Cell Signaling Technology	Cat# 3777S; RRID: AB_2096270
Phospho-ERK1/2 (Thr202/Tyr204) rabbit monoclonal antibody	Cell Signaling Technology	Cat# 4370S; RRID: AB_2315112
Phospho-MEK1/2 (Ser217/221) rabbit monoclonal antibody	Cell Signaling Technology	Cat# 9154S; RRID: AB_2138017
Phospho-RB (Ser807/811) rabbit monoclonal antibody	Cell Signaling Technology	Cat# 8516S; RRID: AB_11178658

(*Continued on next page*)

Continued

REAGENT or RESOURCE	SOURCE	IDENTIFIER
Phospho-RSK (Ser380) rabbit monoclonal antibody	Cell Signaling Technology	Cat# 11989S; RRID: AB_2687613
PKP3 guinea pig polyclonal customized peptide specific antibody	Peptide Specialty Laboratories	N/A
RB rabbit monoclonal antibody	Cell Signaling Technology	Cat# 9313S; RRID: AB_1904119
RB mouse monoclonal antibody Alexa Fluor® 546	Santa Cruz Biotechnology	Cat# sc-102AF546
RSK1 rabbit monoclonal antibody	Cell Signaling Technology	Cat# 8408S; RRID: AB_10828594
RSK2 rabbit monoclonal antibody	Cell Signaling Technology	Cat# 5528S; RRID: AB_10860075
RSK1/2/3 rabbit monoclonal antibody	Cell Signaling Technology	Cat# 9355S; RRID: AB_659900
RUNX3 mouse monoclonal antibody	Cell Signaling Technology	Cat# 13089S; RRID: AB_2798118
α-tubulin mouse monoclonal antibody	Sigma-Aldrich	Cat# T6199; RRID: AB_477583
β-actin mouse monoclonal antibody	Sigma-Aldrich	Cat# A2228; RRID: AB_476697
Peroxidase AffiniPure Donkey Anti-Guinea Pig IgG	Jackson ImmunoResearch	Cat# 706-035-148; RRID: AB_2340447
Peroxidase AffiniPure Donkey Anti-Mouse IgG	Jackson ImmunoResearch	Cat# 715-035-150; RRID: AB_2340770
Peroxidase AffiniPure Donkey Anti-Rabbit IgG	Jackson ImmunoResearch	Cat# 711-035-152; RRID: AB_10015282
Alexa Fluor® 488 AffiniPure $F(ab')_2$ Fragment Donkey Anti-Guinea Pig IgG	Jackson ImmunoResearch	Cat# 706-546-148; RRID: AB_2340473
Cy™3 AffiniPure $F(ab')_2$ Fragment Donkey Anti-Rabbit IgG	Jackson ImmunoResearch	Cat# 711-166-152; RRID: AB_2313568
Normal rabbit IgG	Santa Cruz Biotechnology	Cat# sc-2027 (discontinued); RRID: AB_737197
Bacterial and virus strains		
E. coli JM109	Promega	Cat# P9751
Chemicals, peptides, and recombinant proteins		
Fetal Bovine Serum (FBS) Superior	Sigma-Aldrich	Cat# S0615
Collagen I, Rat Tail	Corning	Cat# 354236
DMEM, 4.5 g/L high glucose	Sigma-Aldrich	Cat# D6429
DMEM/Ham's F12 (3.5:1.1) medium containing 50 μM $CaCl_2$; customized formulation, w/o: Glucose, w/o: L-Glutamine, w/o:Phenol red, w/o: Sodium pyruvate, w: 3.096 g/L $NaHCO_3$	Pan-Biotech	N/A
Chelex 100 Chelating Resin	Bio-Rad	Cat# 142-2842
Sodium pyruvate solution, 100 mM	Sigma-Aldrich	Cat# S8636
Ala-Gln solution, 200 mM	Sigma-Aldrich	Cat# G8541
Adenine	Sigma-Aldrich	Cat# A8626-5G
Hydrocortisone	Sigma-Aldrich	Cat# H4001-1G
Insulin solution	Sigma-Aldrich	Cat# I9278
Epidermal growth factor	Sigma-Aldrich	Cat# E4127
Choleratoxin	Sigma-Aldrich	Cat# C8052
D-(+)-Glucose solution, 45%	Sigma-Aldrich	Cat# G8769
Puromycin dihydrochloride from *Streptomyces alboniger*	Sigma-Aldrich	Cat# P8833
Xfect™ Transfection Reagent	Takara Bio	Cat# 631318
Lipofectamine® RNAiMax	Thermo Fisher Scientific	Cat# 13778150
Trypsin (2.5%)	Thermo Fisher Scientific	Cat# 15090046

(*Continued on next page*)

Continued

REAGENT or RESOURCE	SOURCE	IDENTIFIER
Gefitinib	Sigma-Aldrich	Cat# SML1657
Dimethyl sulfoxide (DMSO)	Sigma-Aldrich	Cat# D2650-100ML
Lambda Phosphatase	New England Biolabs	Cat# P0753L
RNase A	Sigma-Aldrich	Cat# 10109142001
Propidium iodide	Thermo Fisher Scientific	Cat# P3566
Halt™ protease and phosphatase inhibitor cocktail	Thermo Fisher Scientific	Cat# 78444
Benzonase	Santa Cruz Biotechnology	Cat# sc-202391
Pierce™ Protein A Plus Agarose	Thermo Fisher Scientific	Cat# 22811
GFP-Trap Agarose	Chromotek	Cat# gta-20
Western Blot Ultra-Sensitive HRP Substrate	Takara Bio	Cat# T7104A
SuperScript® II Reverse Transcriptase	Thermo Fisher Scientific	Cat# 18064014
Random hexamer primers	Thermo Fisher Scientific	Cat# SO142
2x QPCR SYBRGreen Master Mix	Steinbrenner-Laborsysteme GmbH	Cat# SL-9902
Hoechst 33342	Thermo Fisher Scientific	Cat# H1399
Mowiol® 4-88	Sigma-Aldrich	Cat# 81381
1,4- diazabicyclo[2.2.2]octane (DABCO)	Sigma-Aldrich	Cat# D27802
Lenti-X concentrator	Takara Bio	Cat# 631232
Critical commercial assays		
Cell Proliferation ELISA, BrdU (colorimetric)	Sigma-Aldrich	Cat# 11647229001
Pierce™ BCA Protein Assay Kit	Thermo Fisher Scientific	Cat# 23225
Experimental models: Cell lines		
Hek293T	Kindly provided by Stefan Hüttelmaier	N/A
WT keratinocytes (murine keratinocytes *PKP3*$^{+/+}$)	Keil et al.[14]	N/A
PKP3-KO keratinocytes (murine keratinocytes *PKP3*$^{-/-}$)	Keil et al.[14]	N/A
WT + PKP3 keratinocytes (murine keratinocytes *PKP3*$^{+/+}$ expressing PKP3-WT-EGFP)	This paper	N/A
WT + GFP keratinocytes (murine keratinocytes *PKP3*$^{+/+}$ expressing EGFP)	This paper	N/A
Oligonucleotides		
qRT-PCR-Primer (Table S4)	This paper	N/A
siPools (Table S1)	siTools Biotech	N/A
Recombinant DNA		
CDK4-HA	van den Heuvel et al.[48]	Addgene plasmid #1876
CDK6-HA	van den Heuvel et al.[48]	Addgene plasmid #1868
pCMV HA hRB-wt	Narasimha et al.[16]	Addgene plasmid #58905
hRB-WT-pEGFP-C2	This paper	N/A
pCMV HA hRBΔCDK	Narasimha et al.[16]	Addgene plasmid #58906
hRBΔCDK-pEGFP-C2	This paper	N/A
Flag-p21-WT	Zhou et al.[49]	Addgene plasmid #16240
pVenus2-HA-C2	Kindly provided by Stefan Hüttelmaier	N/A
p21-WT-pVenus2-HA-C2	This paper	N/A
pMD2.G	Kindly provided by Didier Trono	Addgene plasmid #12259
psPAX2	Kindly provided by Didier Trono	Addgene plasmid #12260
EGFP-pLVX-IRES-puro	This paper	N/A

(*Continued on next page*)

Continued

REAGENT or RESOURCE	SOURCE	IDENTIFIER
PKP3-WT-EGFP-pLVX-IRES-puro	This paper	N/A
FUCCI-pLVX-IRES-puro	Kindly provided by Marcel Köhn	N/A
Software and algorithms		
IncuCyte® S3 Software (version 2021C, Sartorius)	Satorius	https://www.sartorius.com/en/products/live-cell-imaging-analysis/live-cell-analysis-instruments/s3-live-cell-analysis-instrument
MACSQuantify™ Software (version 2.11)	Miltenyi Biotec	Cat# 130-094-556
FlowJo™ Software (version 10.6.0)	BD Biosciences	https://www.flowjo.com/solutions/flowjo/downloads
NIS-Elements AR software (version 4.12.00)	Nikon	https://www.microscope.healthcare.nikon.com/en_EU/products/software/nis-elements
Fiji (ImageJ)	Schindelin et al.[50]	https://imagej.net/software/fiji/downloads
Prism 8.3	GraphPad Software	https://www.graphpad.com/scientific-software/prism/
BioRender	BioRender	https://biorender.com/

RESOURCE AVAILABILITY

Lead contact

Further information and requests for resources and reagents should be directed to and will be fulfilled by the lead contact, Mechthild Hatzfeld (mechthild.hatzfeld@medizin.uni-halle.de).

Materials availability

This study did not generate new unique reagents.

Data and code availability

- All data reported in this paper will be shared by the lead contact upon request.
- This paper does not report original code.
- Any additional information required to reanalyze the data reported in this paper is available from the lead contact upon request.

EXPERIMENTAL MODEL AND SUBJECT DETAILS

Cell lines, cell culture and treatments

HEK293T cells were grown in Dulbecco's modified Eagle's medium [DMEM, 4.5 g/L high glucose, 1 mM sodium pyruvate, 1 mM glutamate, 10% (v/v) fetal calf serum (FCS)] at 37°C in 5% CO_2 and 90% humidity. Immortalized keratinocytes from WT and PKP3-KO mice were described previously.[14] Mouse keratinocytes were grown on 15 μg/mL collagen I (Corning, Glendale, Arizona, USA) in low calcium medium [LCM; DMEM/Ham's F12 medium containing 50 μM $CaCl_2$, 10% (v/v) Ca^{2+}-free FCS, 1 mM sodium pyruvate, 1 mM glutamate, 0.18 mM adenine, 0.5 μg/mL hydrocortisone, 5 μg/mL insulin, 10 ng/mL EGF, 100 pM cholera toxin, 1 mg/mL D-(+)-glucose] at 32°C in 5% CO_2 and 90% humidity.

To generate PKP3-WT keratinocytes expressing EGFP, PKP3-WT-EGFP, as well as PKP3-WT and PKP3-KO keratinocytes expressing FUCCI cell cycle reporter, HEK293 cells were co-transfected by $CaPO_4$ precipitation with the packaging plasmids pMD2.G (Addgene plasmid #12259; gift from Didier Trono), psPAX2 (Addgene plasmid #12260; gift from Didier Trono), and lentiviral expression vector pLVX-IRES-puro encoding EGFP, human PKP3-WT-EGFP[14] or the FUCCI cell cycle reporter (FUCCI-Puro was a gift from M. Köhn). Lentiviral particles were purified 48h after transfection using Lenti-X concentrator (Takara Bio Inc., Kusatsu, Shiga, Japan) according to the manufacturer's protocol. Keratinocytes were incubated with the lentiviral particles for 24h and subsequently selected using puromycin (1 μg/mL) to obtain stable cell lines.

Unless otherwise stated, all experiments were performed in LCM to keep PKP3 in a soluble, cytoplasmic pool in order to analyze its extradesmosomal function. To study the protein expression of differentiation markers and associated cell cycle analyses, LCM was supplemented with 1.2 mM $CaCl_2$ (high calcium medium; HCM) to induce the differentiation of keratinocytes. Unless otherwise stated, cells were seeded at a density of 10,000 cells/cm^2 (low density).

For EGFR inhibition, WT cells were treated with 5 μM gefitinib (Sigma-Aldrich, St. Louis, Missouri, USA) for 24h. Dimethyl sulfoxide (DMSO) was used as a control treatment.

Transfections

Transfection of plasmid DNA was performed using Xfect™ (Takara Bio Inc.) according to the manufacturer's instructions. Keratinocytes were grown in LCM for 24h and incubated with the plasmid-Xfect mixture for 24h.

The siRNA pools (defined pools of 30 selected siRNAs, Table S1) were obtained from siTools Biotech GmbH (Martinsried, Germany) and transfected using Lipofectamine® RNAiMax (Thermo Fisher Scientific, Waltham, MA, USA) according to the manufacturer's instructions. Keratinocytes were transfected in suspension with 2 pmol of the respective siRNA pools and kept in LCM for 72h. Cells were trypsinized, counted, reseeded at a cell density of 10,000/cm^2, and kept in LCM for another 24h.

Plasmids and cloning

Human cDNAs of RBwt and RBΔCDK (pCMV HA hRB-wt and pCMV HA hRB ΔCDK were a gift from Steven Dowdy[16]; Addgene plasmids #58905, #58906) were subcloned into pEGFP-C2 (Takara Bio Inc.). Human cDNA of PKP3 was subcloned into pLVX-IRES-puro (Takara Bio Inc.) containing a C-terminal EGFP-tag. The lentiviral FUCCI-Puro vector was a gift from M. Köhn. Vectors for the production of lentiviral particles pMD2.G and psPAX2 were a gift from Didier Trono (Addgene plasmids #12259, #12260). CDK4-HA and CDK6-HA were a gift from Sander van den Heuvel[48] (Addgene plasmids #1876, #1868). Human cDNA of p21-WT (Flag p21 WT was a gift from Mien-Chie Hung[49]; Addgene plasmid # 16240) was subcloned into pVen2-HA-C2. All constructs were validated by sequencing.

METHODS DETAILS

Cell proliferation assay

For the assessment of cell proliferation in 2D culture, cells were seeded at low density and were grown for up to 96h. Live cell images were automatically taken 4h after seeding and then every 8h by using an IncuCyte® S3 System (Sartorius, Goettingen, Germany) with 20x magnification and the corresponding IncuCyte® S3 Software (version 2021C, Sartorius). For analysis of proliferation, phase images were masked to distinguish between background and nuclei using the basic analyzer provided by the Incucte® S3 Software. Cell proliferation was determined by analyzing the occupied area of individual nuclei over time.

Cell cycle analyses

For cell cycle analyses, were seeded at low density. Cells were harvested by trypsinization at the indicated time points, washed, and fixed overnight in 70% ethanol at −20°C. Cells were pelleted by centrifugation (5 min at room temperature at 3,200 *g*), washed three times with phosphate buffered saline (PBS), and incubated with 40 μg/mL RNAse A (Sigma-Aldrich) containing propidium iodide DNA-staining solution [1 mg/mL sodium citrate, 0.1 mM EDTA, 50 μg/mL propidium iodide (Sigma-Aldrich)] at 37°C for 10 min in the dark. The DNA content of approximately 10,000 cells per sample was measured by flow cytometry using a MACSQuant® flow cytometer and the MACSQuantify™ Software (version 2.11, Miltenyi Biotec, Bergisch-Gladbach, Germany). The results were analyzed using FlowJo™ Software (version 10.6.0, Ashland, OR: Becton, Dickinson and Company).

The FUCCI system was used to analyze the duration of cell cycle phases. Cell cycle phases of WT and PKP3-KO FUCCI cells were monitored based on their fluorescence using an IncuCyte® S3 System with 20x magnification starting 24h after seeding. Live cell images were automatically taken every hour. Individual FUCCI cells were identified and tracked visually for the duration of each phase of the cell cycle using IncuCyte® S3 Software.

BrdU assay

To analyze DNA replication, a colorimetric BrdU assay was performed using the Cell Proliferation ELISA, BrdU Kit (Sigma-Aldrich) according to the manufacturer's instructions. Briefly, 24h, 48h, and 72h after seeding, cells were incubated with BrdU (100 μM) for 6h at 32°C. Cells were fixed for 30 min at room temperature using the fixation solution provided in the kit, incubated with the anti-BrdU peroxidase-coupled antibody for 90 min, and washed three times with PBS to remove unbound antibodies. Tetramethylbenzidine-containing substrate solution was added for 100 min until color development was sufficient for photometric detection. The absorbance of all samples was measured at 370 nm (reference wavelength 492 nm) using a plate reader Infinite® M PLEX (Tecan, Maennedorf, Switzerland). The blank control (assay performed in wells without cells) was subtracted from all other values.

Protein extraction

For protein expression analysis, keratinocytes were lysed in sodium dodecyl sulfate (SDS) buffer [2.5% (v/v) SDS pH 7.5, 1 mM EDTA, 100 mM HEPES; supplemented with 1x Halt™ protease and phosphatase inhibitor cocktail (Thermo Fisher Scientific)] and centrifuged for 15 min at 13,000 *g*. The protein concentration was determined using the Pierce™ BCA Protein Assay Kit (Thermo Fisher Scientific) according to the manufacturer's protocol. Benzonase (Santa Cruz Biotechnology, Dallas, Texas, USA) and SDS-polyacrylamide gel electrophoresis (SDS-PAGE) loading buffer [250 mM Tris/HCl (pH 6.8), 30% (v/v) glycerol, 0.25% (w/v) bromophenol blue, 10% (v/v) β-mercaptoethanol, 8% (v/v) SDS] were added. Samples were heated to 95°C for 5 min, stored at −20°C, separated by SDS-PAGE, and analyzed by immunoblotting.

Nucleus/cytoplasm fractionation

For nucleus/cytoplasm fractionation, 6 × 10^5 keratinocytes were used. All preparation steps were performed on ice. Cells were lysed in hypotonic buffer A [10 mM HEPES (pH 7.9), 10 mM KCl, 0.1 mM EDTA, 0.1 mM EGTA; supplemented with 1x Halt™ protease and phosphatase inhibitor cocktail and 0.5 mM DTT] and incubated for 10 min on an orbital shaker at 600 U/min. NP-40 was added to a final concentration of 3%. The resulting solutions were kept for 10 min. Cells were homogenized using hypodermic needles (0.45 × 25 mm) and up and down passes of the syringe for 10 iterations. Lysates were cleared by centrifugation for 30 s at 4°C and 14,000 *g*. The supernatant was collected as the cytoplasmic fraction and stored at −20°C. The pellet was washed three times in buffer A and incubated in hypertonic buffer C [20 mM HEPES (pH 7.9), 0.42 M NaCl, 1 mM EDTA, 1 mM EGTA; supplemented with 1x Halt™ protease and phosphatase inhibitor cocktail] for 30 min on an orbital shaker at 600 U/min. Lysates were cleared by centrifugation for 30 min at 4°C and 18,000 *g*. The supernatant was collected as the nuclear fraction and stored at −20°C. For SDS-PAGE, cytoplasmic and nuclear fractions were mixed with SDS-PAGE loading buffer. P54nrb and α-tubulin were used as positive controls for the nuclear and cytoplasmic fractions, respectively.

Immunoprecipitation

For each immunoprecipitation (IP) reaction, 6 × 10^5 keratinocytes were used. All steps were performed on ice. Cells were lysed in IP-buffer [20 mM Tris-HCl pH 7.5, 137 mM NaCl, 2 mM EDTA, 10% (v/v) glycerol, 1% (v/v) NP-40; supplemented with 1x Halt™ protease and phosphatase inhibitor cocktail]. Lysates were cleared by centrifugation for 15 min at 4°C and 13,000 *g*. One-sixth of the lysate was mixed with SDS-PAGE loading buffer and stored at −20°C as an input control. The residual lysate was incubated with anti-E2F1 (Abcam, Cambridge, UK) antibody overnight at 4°C on an overhead rotator. Normal rabbit IgG (Santa Cruz) was used as an isotype control. Protein A agarose beads (Thermo Fisher Scientific) were washed in IP buffer and added to the lysate for 1h at 4°C on an overhead rotator. Lysates were centrifuged for 3 min at 4°C and 4,000 *g*, washed three times in IP buffer, and bound proteins eluted in SDS-PAGE loading buffer.

For GFP-Trap experiments, cells expressing a GFP-tagged protein were treated as described above. The obtained cell lysates were incubated with GFP-Trap Agarose (ChromoTek, Planegg, Germany) for 1h at 4°C on an overhead rotator, washed as described above, and eluted in SDS-PAGE loading buffer. In either case, input and eluate samples were separated by SDS-PAGE and analyzed by immunoblotting.

Validation of P-RB-Ser807/811 antibody

For validation of RB phosphorylation, WT keratinocytes were lysed in IP-buffer [20 mM Tris-HCl pH 7.5, 137 mM NaCl, 2 mM EDTA, 10% (v/v) glycerol, 1% (v/v) NP-40]. 80 μL of cleared WT cell lysates were mixed with 20 μL Lambda PP-buffer [50 mM HEPES (pH 7.5), 100 mM NaCl, 2 mM DTT, 0.01% Brij 35, supplemented with 1 mM $MnCl_2$] and incubated with or without 4 μL Lambda phosphatase (PP) (New England Biolabs, Frankfurt, Germany) at 30°C for 30 min on an orbital shaker at 900 U/min. Subsequently, SDS-PAGE loading buffer was added and samples were separated by SDS-PAGE and analyzed by immunoblotting.

SDS-PAGE and immunoblotting

Equal amounts of protein were separated by SDS-PAGE. Proteins were transferred to Amersham™ Protan™ nitrocellulose blotting membranes (pore size 0.2 μm, Th. Geyer, Renningen, Germany) using Mini Trans-Blot cells (Bio-Rad Laboratories, Hercules, California, USA). After transfer, membranes were stained in Ponceau S solution [0.2% (w/v) Ponceau S, 3% (w/v) TCA, 3% (w/v) sulfosalicylic acid] for 5 min, washed in distilled water, and documented using a scanner. Membranes were cut, destained in Tris-buffered saline with Tween 20 (TBST), blocked with 3% (w/v) skimmed milk/TBST or 3% (w/v) bovine serum albumin (BSA)/TBST, and subsequently probed overnight with the appropriate primary antibodies as listed in Table S2. Membranes were washed three times with TBST and incubated for 1h with the appropriate horseradish peroxidase-conjugated secondary antibodies (Dianova, Hamburg, Germany, see Table S3). Membranes were treated with ECL Western Blotting Substrate [equal parts chemiluminescence solution 1 (100 mM Tris/HCl [pH 8.5], 25 mM luminol, 0.4 mM coumaric acid) and 2 (100 mM Tris/HCl [pH 8.5], 0.02% [v/v] H_2O_2)] or Western Blot Ultra-Sensitive HRP Substrate (Takara) and chemiluminescence detected using a Fusion-SL 3500WL imaging system (Peqlab, Erlangen, Germany). If staining with additional antibodies was required, the membranes were washed three times in TBST for 10 min each, incubated in stripping buffer [0.2 M glycine, 0.05% tween 20 (pH 2.5)] for 1h, washed again in TBST (3 × 10 min), blocked, and treated with antibodies as described above. β-actin or Ponceau S staining was used as the loading control.

RNA expression

Total RNA was isolated from keratinocytes grown 72h in LCM. Cells were homogenized in Trizol and RNA isolated by phenol/chloroform extraction and isopropanol precipitation.

For cDNA synthesis, 1 μg total RNA served as the template using SuperScript II Reverse Transcriptase (Thermo Fisher Scientific) and random hexamer primers following the manufacturer's protocol. Real-time PCR was performed with primaQUANT 2x qPCR CYBR Green MasterMix w/o ROX (Steinbrenner-Laborsysteme GmbH, Wiesenbach, Germany) using a LightCycler 480 II Real-Time PCR system (Roche, Basel, Switzerland) with the following PCR conditions: 95°C for 15 min followed by 40 cycles of 95°C for 15 s, 62°C for 15 s, and 72°C for 20 s. Primer pairs were selected using Primer Blast (https://www.ncbi.nlm.nih.gov/tools/

primer-blast/). The primer sequences are listed in Table S4. The relative abundance of RNA was determined by the $\Delta\Delta C_t$ method and calculated by the following formula: ratio = $(E_{target})^{\Delta CT_{target}}/(E_{reference})^{\Delta CT_{reference}}$. *Eif3k* mRNA was used as a reference.

Immunofluorescence analysis and image processing

Cells were grown on 12-mm collagen I-coated glass coverslips and fixed for 10 min in 3.7% (w/v) formaldehyde in PBS on ice, permeabilized in detergent buffer [100 mM PIPES(pH 6.9), 4 M glycerol, 2 mM EDTA, 1 mM EGTA, 0.5% (v/v) Triton X-100] for 15 min at room temperature, and blocked in 1% (w/v) BSA/PBS for 30 min at room temperature. Primary antibodies were diluted in blocking solution and incubated overnight at 4°C in a humid chamber. The next day, coverslips were washed in PBS, briefly blocked, and incubated for 1h at room temperature with the fluorophore-conjugated secondary antibody. DNA was stained with Hoechst 33342 (Thermo Fisher Scientific). Antibodies used for immunofluorescence are listed in Table S2 and Table S3. Coverslips were mounted in Mowiol [5% (w/v) Mowiol, 30% (v/v) glycerol, 0.25% (w/v) 1,4- diazabicyclo[2.2.2]octane (DABCO)]. Images were taken using a Nikon Eclipse E600 microscope, a CCD camera, and a Plan APO 60xA/1.40 oil objective controlled by the NIS-Elements AR software (version 4.12.00). For comparisons between WT and PKP3-KO cells, samples were treated in parallel and images captured at the same exposure times. Fiji software was used for image processing.[50]

QUANTIFICATION AND STATISTICAL ANALYSIS

Immunoblot quantification

For quantification of immunoblots, we used the ImageJ tool ''Gel Analysis''. All signals were normalized to the internal loading control β-actin. If β-actin expression varied due to experimental conditions, Ponceau S staining was used as the loading control. Details concerning normalization procedures are given in the figure legends.

Quantification of immunofluorescence

To determine the enrichment factors for RB and CDKN1A in the nucleus and cytoplasm, fluorescence intensities were measured in segments of equal length (100 pixels) and width (40 pixels) across individual nuclei as illustrated in Figure S6. All nuclei of the entire image were evaluated with the exception of mitotic, polynuclear, or overgrowing cells. Each line scan resulted in a histogram depicting the fluorescence intensities along the bar. The enrichment factors for RB were calculated by dividing the mean cytoplasmic value (50-pixel length at the end of the 100-pixel scan line) by the mean nuclear value (50-pixel length at the start of the 100-pixel scan line) for each line scan. To quantify CDKN1A fluorescence intensities, the mean nuclear value was divided by the mean cytoplasmic value. At least 250 cells were analyzed per condition from two independent experiments.

Statistical analysis

Statistical analysis and plot preparation were performed using Graphpad Prism Software (version 8.3). All individual data points are shown in the plots. Boxplots display the first to third quartile; whiskers extend to the minimum and maximum. For two independent datasets, significant differences were determined by a two-tailed Student's t-test. To compare more than two independent datasets with normal distribution, one-way analysis of variance (ANOVA) followed by a Tukey's multiple comparison test was used.